International Journal of Solids and Structures 301 (2024) 112943

Contents lists available at ScienceDirect

International Journal of Solids and Structures

journal homepage: www.elsevier.com/locate/ijsolstr

Safety assessment of masonry undamaged and damaged arches subjected to gravitational loads and horizontal forces. A numeric procedure to identify the optimal thrust line

Stefano Galassi [a,*], Giacomo Tempesta [b]

[a] Department of Architecture, University of Florence, Florence, Italy
[b] Department of Architecture, UKZKM, Nostra Signora del Buon Consiglio, Tirana, Albania

ARTICLE INFO

Keywords:
Undamaged and damaged arches
Masonry
Optimal thrust line
Minimization procedure
Safety assessment

ABSTRACT

In 2019 the authors formulated a numerical procedure for assessing the safety of masonry arches based on their geometry and the shape of the thrust line. The thrust line is calculated to be nearest to the geometric axis of the arch, because it is that corresponding to the optimal inner stress state. The original procedure, which focused on the safety analysis of undamaged fixed arches subject to gravitational loads, is reformulated here to also consider arches on pinned supports as well as damaged arches, i.e. one- and two-hinged arches. The procedure is further extended to also assess safety against horizontal actions, such as those resulting from an earthquake. Finally, safety is evaluated by identifying the domain of admissible thrust lines within the thickness of the arch and by computing the degree of safety in terms of the capacity of the thrust line to be moved vertically within the domain. The reformulation and extension of the procedure exploits the technique of partitioned matrices to enable automation and easy implementation in structural calculation software.

1. Introduction

The equilibrium analysis of the masonry arch is a statically indeterminate problem. This problem was often solved by searching for any thrust line within the arch profile to ensure safety. In the 19th century the emerging theory of elasticity shifted interest toward finding the actual inner stress state, that is, the true line of thrust. To find it, the hypothesis of rigid body must be removed and the inertial and elastic characteristics of the arch must be considered to establish the congruency or compatibility conditions.

To circumvent the static indeterminacy of the equilibrium problem (Paradiso et al., 2014) and to avoid considering the mechanical properties of the masonry and its effective deformability, many researchers have proposed, recently and in the past, methods based only on the equilibrium analysis. In this regard, it is worth recalling E. Mèry (1840), who proposed in the nineteenth century a fully graphic method of drawing the line of thrust of symmetric arches which is affected by the elasticity theory only in the position of the centers of pressure (Navier's middle-third rule). More recently, the eighteenth-century theories, focused on the analysis of arches considered made of rigid blocks without mortar at the joints, were revisited in terms of limit analysis (Del Piero, 1998; Drucker et al., 1952; Heyman, 1966; Livesley, 1978; Gilbert, 2001; Marmo, 2021; Riveiro et al., 2011). In this context two approaches are used: the thrust line method (Block et al., 2006; Briccoli Bati et al., 2013; Huerta, 2001; Livesley, 1978; Como and Sinopoli, 1998; Galassi, 2023), based on the lower bound theorem of limit analysis, and the mechanism method (Cavalagli et al., 2016, Dimitri and Tornabene, 2015; Gilbert, 2007; Grillanda et al., 2023; Ng and Fairfield, 2004; Iannuzzo et al., 2021; Milani et al., 2008; Smars, 2010; Stockdale et al., 2018; Zampieri et al., 2018a, 2018b, 2019a, 2019b), based on the upper bound theorem. These methods provide a measure of the safety of arches at Ultimate Limit State based on calculating the collapse factor of an additional load. In recent decades, thrust line methods, which assess the safety of an arch by checking whether the shape of the thrust line fits that of the arch profile within which it is to be contained, were also applied to the analysis of vaults, by searching for the existence of any compression-only force network within the boundaries of the vault (Block and Ochsendorf, 2007; Marmo and Rosati, 2017; Marmo et al., 2019; O'Dwyer, 1999).

To get around the static indeterminacy, Moseley (1833) enunciated a new principle in Statics, called "principle of least pressure", according to which the true line of thrust is that which minimizes the horizontal

* Corresponding author.
E-mail addresses: stefano.galassi@unifi.it (S. Galassi), g.tempesta@prof.unizkm.al (G. Tempesta).

https://doi.org/10.1016/j.ijsolstr.2024.112943
Received 20 April 2024; Received in revised form 10 June 2024; Accepted 20 June 2024
Available online 23 June 2024
0020-7683/

thrust at the key. This principle would lead to the conclusion that if an arch is symmetric and subject only to vertical loads, the horizontal thrust being constant in all cross sections of the arch, the true line of thrust is that which passes through the extrados point of the key section and the intrados points of the sections at the haunches. Later Winkler (1867), recalling this principle, stated that the true line of thrust is the one nearest to the centroidal axis of the arch. No one has ever demonstrated that this is the true line of thrust; however, it is undoubtedly the best line of thrust because it is the one that corresponds to a quite uniform compressive stress and the lowest shear and bending stresses in the cross sections of the arch.

In relation to this topic, it is worth mentioning that, in the past, some authors developed methods for designing arches so that their geometric axis complied with that of the thrust line. Yvon Villarceau (1854) proposed an analytical method to determine the intrados profile of an arch so that the centroidal axis, obtained by connecting the centroids of the blocks, corresponds to the line of thrust of the loads, because it was believed to be the one that provided the safest profile of an arch. Regarding this statement, it is worth mentioning that Gregory (1967) was the first to argue that the best shape of an arch to support itself is that of a catenary form and provided the mathematical equation for it. Next, Fuller (1875), mentioning a previous study published by Bell (1872), tackled the same topic as Villarceau by developing an entirely graphic method for detecting the equilibrium curve for a rigid arch rib subjected to gravitational loads. Afterwards, in the 20th century Inglis (1951) developed an equation representing a set of curves (namely centroidal axes) for the design of arches carrying an upper roadway.

All these authors shared a common hypothesis: the arch they refer to is the classic Roman arch, with radial (Vitruvian) joints. Indeed, if joints have a different inclination, i.e. a different stereotomy is considered, the line of thrust nearest to the geometric axis could even not be the safest one and, certainly, the inner stress state at joints is different. In particular, also the profile of the thrust line is affected by the stereotomy, as clearly shown by Heyman (2009) and numerically analyzed by Makris and Alexakis (2013) for prefixed stereotomy patterns and by Gáspár et al. (2018) which considered a stereotomy function.

Conversely, the opposite topic of assessing safety (i.e. verification problem) of existing masonry arches on the basis of the shape of the thrust line nearest to the geometric axis is not much investigated in present and past literature. This topic was dealt with, firstly, by Heyman in 1969 who developed an iterative method that found an approximate solution to the problem and, successively, by us in 2019 who provided the exact mathematical solution (Tempesta and Galassi, 2019).

In all the aforementioned procedures based on the thrust line nearest to the geometric axis, only undamaged fixed arches subject to gravitational loads are considered, i.e. statically indeterminate structures to third degree. However, the arches may have been constructed with geometric imperfections, with a nonhomogeneous material (Gusella et al., 2019), or may have suffered damage during their life cycle. Thus, at the imperfect or cracked sections hinges can have opened. To the best of the authors' knowledge, no one before has tackled the safety of cracked arches by exploiting a technique based on the line of thrust nearest to the geometric axis. In the paper the numerical procedure for detecting the line of thrust nearest to the geometric axis of undamaged arches proposed by the authors is extended here to consider one- and two-hinged arches as well. Arches on pinned supports are also analyzed. The occurrence of the hinges at inner joints or at the pinned supports requires that the thrust line passes through the hinges, a circumstance that reduces the degree of static indeterminacy. Furthermore, to assess safety against the horizontal actions caused by an earthquake, the procedure is extended to also indirectly implement, without inputting in the arch model horizontal forces proportional to the gravitational loads, the effect of these forces by taking advantage of the analogy between a structure placed on a rigid inclined platform and the inclined action lines of the resultant vectors of the gravitational loads and horizontal seismic forces acting on the structure at its actual position.

The paper is arranged as follows: this introductory section briefly retraces the state-of-the art on the subject under consideration; Section 2 discusses the numerical procedure developed to detect the line of thrust nearest to the geometric axis of an arch both undamaged, with two cases of constraint at the abutments (fixed and pinned supports), and damaged, the damage being interpreted as inner hinges. The same section also presents the technique for implementing horizontal loads in the procedure by exploiting the analogy with the inclined platform. Section 3 is devoted to assessing the safety of the arch, based on comparing the shape of the line of thrust detected with the intrados and extrados profiles of the arch. The domain of safety which provides the degree of safety of the arch against gravitational and horizontal loads, is identified. In Section 4 some numerical case studies are analyzed using the proposed procedure. The paper ends with Section 5, where the main conclusions are drawn.

2. Numerical procedure

The goal of the procedure is assessing the safety of masonry arches against gravitational loads and horizontal forces on the theoretical basis of geometric considerations. Following Heyman's theory (Heyman, 1969), for which collapse in masonry arches is generally due to structural shapes unsuitable to support the assigned loads rather than to the material strength being exceeded, the procedure compares the shape of the thrust line with the shape of the arch and computes the degree of safety. Among the thrust lines within the arch profile which assure safety according to the Heyman's master safe theorem (Heyman, 1966), the procedure searches for the thrust line nearest to the geometric axis, which can be considered, from the Heyman's point of view, the safest one because it is that which provides the highest geometrical factor of safety (as it identifies the ideal arch of minimum thickness within the profile of the arch), obviously under the assumption that stereotomy is not considered. Instead, if stereotomy, i.e. the bricklaying pattern, is also considered, the issue is more subtle because the thrust line intersects the joints at points that depend on the inclination of the joints, and, as a result, the thrusts transferred from one block to another through their joints also decompose into axial compressive and shear forces that depend on the inclination of the joints. Notwithstanding that the bending moment at the joint centroids is not affected by stereotomy and is in any case of minimum value if the thrust line is the nearest one to the geometric axis, this thrust line may not even be the safest for all conditions of stereotomy, because of the shearing forces which could be so high as to cause the sliding of blocks. In addition, the thrust line nearest to the geometric axis is also safer than that provided by the limit analysis because, as it never touches the intrados and extrados, it never identifies joints where stress is theoretically infinite and capable of crushing masonry, and where hinges, capable of triggering collapse mechanisms, can open. It is worth noting that in the proposed procedure the arch analyzed is a continuous structure and, therefore, stereotomy affects neither the profile of the thrust line nor the safety verification. This aspect also differentiates the proposed procedure from procedures and software developed specifically for the analysis of rigid-block models (Livesley, 1978; Gilbert, 2001, 2007), where the arrangement of bricks and joints affects the failure mode, notwithstanding that our procedure can also be applied to discrete models.

The numerical technique to detect the thrust line nearest to the geometric axis exploits the finite difference method. The distances between the vertices of the thrust line and the intersection points between the lines of action of loads and the geometric axis are minimized computing the square or such distances in order to make the negative distances irrelevant in the minimization procedure.

With a single procedure, which exploits the technique of partitioned matrices, both undamaged and damaged arches can be analyzed. Fixed arches and arches on pinned supports are the undamaged arches under investigation. Damaged arches are modelled as one- or two-hinged arches, through which the thrust line mast pass. The case of the three-

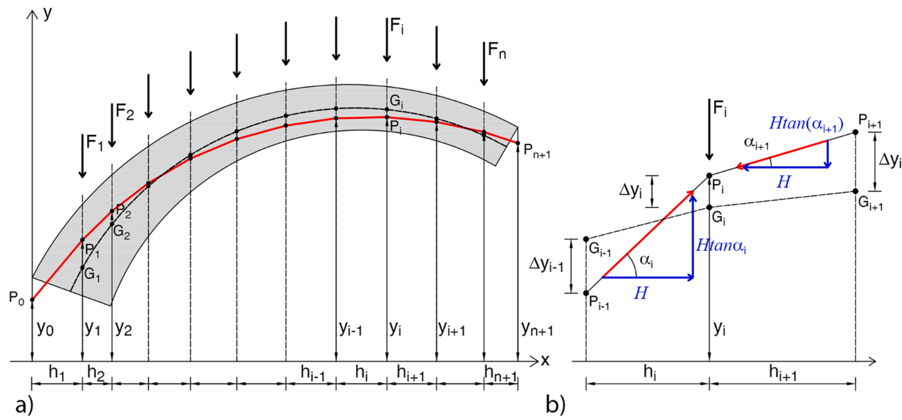

Fig. 1. a) Reference fixed arch model; b) detail of vertex 'i' of the thrust line.

hinged arch is worthless because the thrust line passing through the three hinges is only one. The procedure applies to different load cases: vertical (gravitational) loads, horizontal loads proportional to the gravitational ones and incremental point forces.

A closed-form solution is provided for undamaged arches, while for damaged arches the procedure must be reiterated, and the solution is provided for trials and errors.

Shortly, the following steps are performed to assess the safety of arches:

- Computation of the thrust line nearest to the geometric axis of the arch;
- Identification of the domain of safety, which is a region that contains all the admissible lines of thrust parallel to the nearest one to the geometric axis and contained within the profile of the arch;
- Computation of the degree of safety of the arch.

2.1. Undamaged arch

2.1.1. The fixed arch

Let us consider a masonry arch fixed to its supports. Let the arch of Fig. 1a be a continuous arch, identified by the profile of the geometric axis, intrados and extrados and subject to the discrete set of gravitational loads F_1, F_2, F_3, …, F_n. Let us apply the loads F_i (with $1 \leq i \leq n$) to the intersection points G_i between their lines of action and the geometric axis. According to Villarceau (1954), points G_i are the centroids of the reference sections of the arch and the geometric axis corresponds to the centroidal arches. It is worth noting that the arch of Fig. 1a can represent a rigid-block arch as well: in such a case, points G_i identify the centroids of the blocks and the geometrical axis of the arch is the polyline which passes through points G_i.

Given any system of forces, the funicular polygons that can be drawn are infinite and this infinity depends on three free variables which are, in Graphic Statics, the position of the pole in the force polygon (i.e.: its two coordinates) and the height of the sides of the funicular polygon. Based on this, a set of ∞^3 funicular polygons can be traced for the assigned load case, each representing a different state of equilibrium between external loads and support reactions. Moreover, since these funicular polygons indicate the path of inner forces throughout the arch, they are the *polygons of the successive resultant vectors* and, consequently, are also called *thrust lines*.

To identify a specific thrust line, three parameters or conditions must be set forth. We assign the ordinates of points $P_0 \equiv (x_0, y_0)$ and $P_{n+1} \equiv (x_{n+1}, y_{n+1})$, at which the first and the last side of the thrust line must pass, and the horizontal thrust H.

To approach the problem and identify the vertices of the thrust line, the equilibrium condition of the vertical components of the inner forces and external loads applied to the vertices is written. Referring to the i-th vertex $P_i \equiv (x_i, y_i)$ of the thrust line shown in Fig. 1b, the equilibrium condition is given by Eq. (1):

$$(\tan\alpha_i - \tan\alpha_{i+1}) = \frac{F_i}{H} \tag{1}$$

where α_i and α_{i+1} are the inclination angles of the two sides of the thrust line connected to the vertex i and F_i is the i^{th} gravitational load. Expressing the tangents of angles α_i and α_{i+1} in the form of Eq. (2):

$$\begin{aligned} \tan\alpha_i &= \frac{Y_i - Y_{i-1}}{h_i} \\ \tan\alpha_{i+1} &= \frac{Y_{i+1} - Y_i}{h_{i+1}} \end{aligned} \tag{2}$$

where $h_i = (x_i - x_{i-1})$ and $h_{i+1} = (x_{i+1} - x_i)$ are the distances between the lines of action of successive gravitational loads F_{i-1}, F_i, F_{i+1}, the equilibrium equation expressed by Eq. (1) takes the expression of Eq. (3):

$$\left(\frac{-1}{h_i}\right)\cdot y_{i-1} + \left(\frac{h_i + h_{i+1}}{h_i \cdot h_{i+1}}\right)\cdot y_i + \left(\frac{-1}{h_{i+1}}\right)\cdot y_{i+1} = \frac{F_i}{H} \tag{3}$$

The extension of Eq. (3) to all vertices of the thrust line leads to the system of n linear equations in $n + 3$ unknowns that follows:

$$\begin{cases} \left(\frac{-1}{h_1}\right)\cdot y_0 + \left(\frac{h_1 + h_2}{h_1 \cdot h_2}\right)\cdot y_1 + \left(\frac{-1}{h_2}\right)\cdot y_2 = \frac{F_1}{H} \\ \left(\frac{-1}{h_2}\right)\cdot y_1 + \left(\frac{h_2 + h_3}{h_2 \cdot h_3}\right)\cdot y_2 + \left(\frac{-1}{h_3}\right)\cdot y_3 = \frac{F_2}{H} \\ \dots\dots\dots\dots\dots\dots\dots\dots\dots\dots \\ \left(\frac{-1}{h_i}\right)\cdot y_{i-1} + \left(\frac{h_i + h_{i+1}}{h_i \cdot h_{i+1}}\right)\cdot y_i + \left(\frac{-1}{h_{i+1}}\right)\cdot y_{i+1} = \frac{F_i}{H} \\ \dots\dots\dots\dots\dots\dots\dots\dots\dots\dots \\ \left(\frac{-1}{h_n}\right)\cdot y_{n-1} + \left(\frac{h_n + h_{n+1}}{h_n \cdot h_{n+1}}\right)\cdot y_n + \left(\frac{-1}{h_{n+1}}\right)\cdot y_{n+1} = \frac{F_n}{H} \end{cases} \tag{4}$$

In Eq. (4) the ordinates y_i of the $n + 2$ vertices of the thrust line and the horizontal thrust H are the unknowns to be computed. This equation shows the static indeterminacy to third degree of the arch equilibrium problem.

Taking the three parameters set forth above as the three redundant unknowns and putting $k = \frac{1}{H}$, the system of Eq. (4) is rearranged, in matrix form, to separate the three redundant parameters (k, y_0, y_{n+1}) from the general system as follows:

$$\begin{bmatrix} \left(\frac{h_1+h_2}{h_1 \cdot h_2}\right) & \left(\frac{-1}{h_2}\right) & 0 & 0 \\ \left(\frac{-1}{h_2}\right) & \left(\frac{h_2+h_3}{h_2 \cdot h_3}\right) & \left(\frac{-1}{h_3}\right) & 0 \\ \cdots & \cdots & \cdots & \cdots \\ 0 & \left(\frac{-1}{h_i}\right) & \left(\frac{h_i+h_{i+1}}{h_i \cdot h_{i+1}}\right) & \left(\frac{-1}{h_{i+1}}\right) \\ \cdots & \cdots & \cdots & \cdots \\ 0 & 0 & \left(\frac{-1}{h_n}\right) & \left(\frac{h_n+h_{n+1}}{h_n \cdot h_{n+1}}\right) \end{bmatrix} \cdot \begin{Bmatrix} y_1 \\ y_2 \\ \cdots \\ y_i \\ \cdots \\ y_n \end{Bmatrix} = \begin{Bmatrix} F_1 \\ F_2 \\ \cdots \\ F_i \\ \cdots \\ F_n \end{Bmatrix} \cdot k + \begin{Bmatrix} \frac{1}{h_1} \\ 0 \\ \cdots \\ 0 \\ \cdots \\ 0 \end{Bmatrix} \cdot y_0 + \begin{Bmatrix} 0 \\ 0 \\ \cdots \\ 0 \\ \cdots \\ \frac{1}{h_{n+1}} \end{Bmatrix} \cdot y_{n+1} \tag{5}$$

or, more compactly, as:

$$[\mathrm{D}]\{\mathrm{Y}\} = \{\mathrm{T}_1\} \cdot \mathrm{k} + \{\mathrm{T}_2\} \cdot \mathrm{y}_0 + \{\mathrm{T}_3\} \cdot \mathrm{y}_{n+1} \tag{6}$$

where:

- $[\mathrm{D}] \in \Re^{n \cdot n}$ is the matrix of the coefficients of the unknowns;
- $\{\mathrm{Y}\} \in \Re^{n}$ is the vector collecting the ordinates of the vertices of the thrust line, i.e. the unknowns of the equilibrium problem;
- $\{\mathrm{T}_1\} \in \Re^{n}$ is the vector whose components are the magnitudes of loads $\mathrm{F_i}$;
- $\{\mathrm{T}_2\} \in \Re^{n}$ is a vector whose only nonzero component is the coefficient $\frac{1}{h_1}$ of the unknown y_0;
- $\{\mathrm{T}_3\} \in \Re^{n}$ is a vector whose only nonzero component is the coefficient $\frac{1}{h_{n+1}}$ of the unknown y_{n+1}.

It is worth noting that matrix [D] is a symmetric band matrix and, therefore, is easy to build automatically.

Putting $\{\mathrm{R}_1\} = [\mathrm{D}]^{-1}\{\mathrm{T}_1\}$, $\{\mathrm{R}_2\} = [\mathrm{D}]^{-1}\{\mathrm{T}_2\}$, $\{\mathrm{R}_3\} = [\mathrm{D}]^{-1}\{\mathrm{T}_3\}$, the solution of Eq. (6) provides vector {Y}:

$$\{\mathrm{Y}\} = \{\mathrm{R}_1\} \cdot \mathrm{k} + \{\mathrm{R}_2\} \cdot \mathrm{y}_0 + \{\mathrm{R}_3\} \cdot \mathrm{y}_{n+1} \tag{7}$$

The conditions of invertibility of matrix [D] are discussed in Appendix C.

The components of vector {Y}, given by Eq. (7), are the ordinates of the vertices of all ∞^3 thrust lines of the loads stored in vector T_1, as a function of the three redundant unknowns chosen above.

Thus, since the goal of the procedure is detecting the thrust line nearest to the geometric axis of the arch, the three redundant unknowns must be computed to meet the “nearness” requirement above. To compute them, a procedure is formulated to minimize the vertical distances of the vertices of the thrust line being researched from the centroids $\mathrm{G_i}$.

To nullify the effect of the sign of these distances in the minimization procedure, the square of the differences Δy_i between the ordinates y_i of the vertices P_i of the thrust line and the ordinates y_Gi of the centroids G_i is calculated and denoted as function S in Eq. (8):

$$\mathrm{S} = \sum_{\mathrm{i}=1}^{\mathrm{n}} (\Delta y_\mathrm{i})^2 = \sum_{\mathrm{i}=1}^{\mathrm{n}} (y_\mathrm{i} - y_\mathrm{Gi})^2 \tag{8}$$

Putting $\{\mathrm{Y_G}\} \in \Re^{n}$ the vector collecting the ordinates of the centroids G_i on the geometric axis and recalling Eq. (7), Eq. (8) is rewritten, in matrix form, as:

$$\mathrm{S} = (\{\mathrm{Y}\} - \{\mathrm{Y_G}\})^2 = (\{\mathrm{R}_1\} \cdot \mathrm{k} + \{\mathrm{R}_2\} \cdot \mathrm{y}_0 + \{\mathrm{R}_3\} \cdot \mathrm{y}_{n+1} - \{\mathrm{Y_G}\})^2 \tag{9}$$

To minimize the function S, its partial derivatives are calculated with respect to the three redundant unknowns and set equal to zero:

$$\begin{aligned} \frac{\partial \mathrm{S}(\mathrm{k}, \mathrm{y}_0, \mathrm{y}_{n+1})}{\partial \mathrm{k}} &= 0 \\ \frac{\partial \mathrm{S}(\mathrm{k}, \mathrm{y}_0, \mathrm{y}_{n+1})}{\partial \mathrm{y}_0} &= 0 \\ \frac{\partial \mathrm{S}(\mathrm{k}, \mathrm{y}_0, \mathrm{y}_{n+1})}{\partial \mathrm{y}_{n+1}} &= 0 \end{aligned} \tag{10}$$

Eq. (10) represents the necessary conditions for a point to be a stationary point. The proof that this is the minimum of the function S is given in Appendix C, where the sufficient condition is also discussed.

The solution of Eq. (10) leads to the system of three linear equations in three unknowns shown in Eq. (11):

$$\begin{cases} \{\mathrm{R}_1\}^2 \cdot \mathrm{k} + \{\mathrm{R}_1\}\{\mathrm{R}_2\} \cdot \mathrm{y}_0 + \{\mathrm{R}_1\}\{\mathrm{R}_3\} \cdot \mathrm{y}_{n+1} - \{\mathrm{R}_1\}\{\mathrm{Y_G}\} = \{0\} \\ \{\mathrm{R}_2\}^2 \cdot \mathrm{y}_0 + \{\mathrm{R}_1\}\{\mathrm{R}_2\} \cdot \mathrm{k} + \{\mathrm{R}_2\}\{\mathrm{R}_3\} \cdot \mathrm{y}_{n+1} - \{\mathrm{R}_2\}\{\mathrm{Y_G}\} = \{0\} \\ \{\mathrm{R}_3\}^2 \cdot \mathrm{y}_{n+1} + \{\mathrm{R}_1\}\{\mathrm{R}_3\} \cdot k + \{\mathrm{R}_2\}\{\mathrm{R}_3\} \cdot \mathrm{y}_0 - \{\mathrm{R}_3\}\{\mathrm{Y_G}\} = \{0\} \end{cases} \tag{11}$$

which, rewritten in matrix form, leads to:

$$\begin{bmatrix} \{\mathrm{R}_1\}^2 & \{\mathrm{R}_1\}\{\mathrm{R}_2\} & \{\mathrm{R}_1\}\{\mathrm{R}_3\} \\ \{\mathrm{R}_1\}\{\mathrm{R}_2\} & \{\mathrm{R}_2\}^2 & \{\mathrm{R}_2\}\{\mathrm{R}_3\} \\ \{\mathrm{R}_1\}\{\mathrm{R}_3\} & \{\mathrm{R}_2\}\{\mathrm{R}_3\} & \{\mathrm{R}_3\}^2 \end{bmatrix} \cdot \begin{Bmatrix} \mathrm{k} \\ \mathrm{y}_0 \\ \mathrm{y}_{n+1} \end{Bmatrix} = \begin{Bmatrix} \{\mathrm{R}_1\}\{\mathrm{Y_G}\} \\ \{\mathrm{R}_2\}\{\mathrm{Y_G}\} \\ \{\mathrm{R}_3\}\{\mathrm{Y_G}\} \end{Bmatrix} \tag{12}$$

that is:

$$[\mathrm{N}]\{\mathrm{P}\} = \{\mathrm{W}\} \tag{13}$$

with $[\mathrm{N}] \in \Re^{3 \cdot 3}$ symmetric matrix, $\{\mathrm{P}\} \in \Re^3$, $\{\mathrm{W}\} \in \Re^3$.

The solution of Eq. (13) gives vector {P}, whose components are the three redundant unknowns:

$$\{\mathrm{P}\} = [\mathrm{N}]^{-1}\{\mathrm{W}\} \tag{14}$$

The conditions of invertibility of matrix [N] are discussed in Appendix C.

The ordinates y_i of the vertices P_i of the thrust line are calculated by entering the values of the three unknowns given by Eq. (14) into Eq. (7), while the abscissas are equal to the abscissas of the centroids G_i.

To plot the thrust line nearest to the geometric axis, vector $\{\mathrm{X}\} \in \Re^{n+2}$ is built and is populated by the abscissa x_0 of point P_0 entered as the first component, then by the abscissas $\mathrm{x_i}$ of the centroids G_i and, finally, by the abscissa x_{n+1} of point P_{n+1} as the last component. Accordingly, vector {Y} is resized coherently with the structure of vector {X} and is populated by the ordinate y_0 of point P_0, the components $\mathrm{y_i}$ of the primitive vector, and the ordinate y_{n+1} of point P_{n+1} (Eq. (15):

$$\{\mathrm{X}\} = \begin{Bmatrix} \mathrm{x}_0 \\ \mathrm{x}_1 \\ \cdots \\ \mathrm{x_i} \\ \cdots \\ \mathrm{x}_{n+1} \end{Bmatrix}, \{\mathrm{X}\} \in \Re^{n+2}, \{\mathrm{Y}\} = \begin{Bmatrix} \mathrm{y}_0 \\ \mathrm{y}_1 \\ \cdots \\ \mathrm{y_i} \\ \cdots \\ \mathrm{y}_{n+1} \end{Bmatrix}, \{\mathrm{Y}\} \in \Re^{n+2} \tag{15}$$

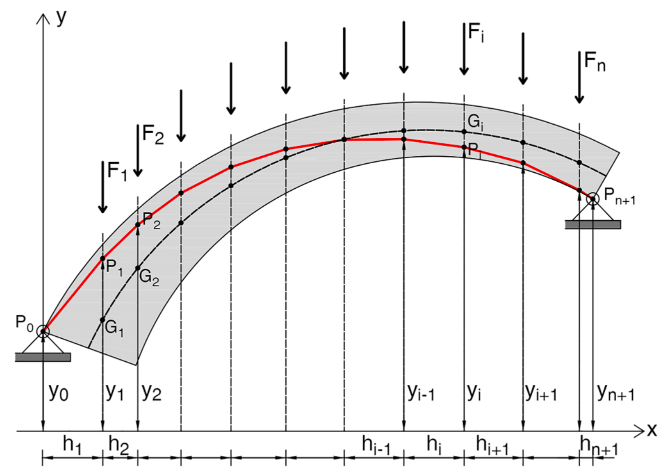

Fig. 2. a) Reference pinned arch model.

The thrust line is drawn by plotting the polyline of vertices (x_i, y_i).

2.1.2. The arch on pinned supports

Let us consider an arch on pinned supports. The right and the left pinned supports are point constrains positioned at the joints of the right and the left imposts. The limit case occurs when the pinned supports are positioned at the intrados or at the extrados of such joints, as illustrated in Fig. 2.

The aim is detecting the thrust line nearest to the geometric axis of the arch obliged passing through the pinned supports. In order to address this problem, points P_0 and P_{n+1} are suitably chosen at the pinned supports. The statically indeterminacy of the problem reduces and becomes equal to first degree, since two conditions are imposed: the first side and the last side of the thrust line must go through point P_0 and P_{n+1}, respectively.

Under these assumptions, it is worth noting that Eqs. (1) to (8) still hold, the function to be minimized is still expressed by Eq. (9) and Eq. (7) gives the ordinates of the vertices of all ∞^1 thrust lines of the loads collected in vector T_1 passing through the pinned supports. However, in the case at hand, the only redundant unknown to be computed is the thrust H or, that is the same, its reciprocal *k*, while the ordinate y_0 of point P_0 (left pinned support) and the ordinate y_{n+1} of point P_{n+1} (right pinned support) are prefixed terms.

To solve this problem and detect the thrust line nearest to the geometric axis, among the ∞^1 thrust lines provided by Eq. (7), function S (Eq. (9) is minimized by setting its derivative, calculated with respect to the unknown *k*, equal to zero. In practice, only the first equation of Eq. (10) still holds and is rewritten as follows:

$$\frac{dS(k)}{dk} = 0 \tag{16}$$

Entering Eq. (9) into Eq. (16) leads to the linear equation that follows:

$$\{R_1\}^2 \cdot k = \{R_1\}\left(\{Y_G\} - \{R_2\} \cdot y_0 - \{R_3\} \cdot y_{n+1}\right) \tag{17}$$

which provides the value of the unknown k:

$$k = \frac{\{R_1\}\left(\{Y_G\} - \{R_2\} \cdot y_0 - \{R_3\} \cdot y_{n+1}\right)}{\{R_1\}^2} \tag{18}$$

The same result (Eq. (18) is more conveniently achieved by partitioning matrices and vectors of Eq. (12) in such a way as to separate components related to the unknown k from components related to the prefixed terms y_0 and y_{n+1}, as indicated in Eq. (19):

$$\begin{bmatrix} \{R_1\}^2 & \{R_1\}\{R_2\} & \{R_1\}\{R_3\} \\ \{R_1\}\{R_2\} & \{R_2\}^2 & \{R_2\}\{R_3\} \\ \{R_1\}\{R_3\} & \{R_2\}\{R_3\} & \{R_3\}^2 \end{bmatrix} \cdot \begin{Bmatrix} k \\ y_0 \\ y_{n+1} \end{Bmatrix} = \begin{Bmatrix} \{R_1\}\{Y_G\} \\ \{R_2\}\{Y_G\} \\ \{R_3\}\{Y_G\} \end{Bmatrix} \tag{19}$$

that is:

$$\begin{bmatrix} N_{1,1} & N_{1,2} \\ N_{2,1} & N_{2,2} \end{bmatrix} \cdot \begin{Bmatrix} P_1 \\ P_2 \end{Bmatrix} = \begin{Bmatrix} W_1 \\ W_2 \end{Bmatrix} \tag{20}$$

where the submatrices of [N] are: $[N_{1,1}] = \left[\{R_1\}^2\right]$, $[N_{1,2}] = [\{R_1\}\{R_2\} \quad \{R_1\}\{R_3\}]$, $[N_{2,1}] = \begin{bmatrix} \{R_1\}\{R_2\} \\ \{R_1\}\{R_3\} \end{bmatrix}$, $[N_{2,2}] = \begin{bmatrix} \{R_2\}^2 & \{R_2\}\{R_3\} \\ \{R_2\}\{R_3\} & \{R_3\}^2 \end{bmatrix}$, the sub-vectors of $\{P\}$ are: $\{P_1\} = \{k\}$, $\{P_2\} = \begin{Bmatrix} y_0 \\ y_{n+1} \end{Bmatrix}$ and the sub-vectors of $\{W\}$ are: $\{W_1\} = \{\{R_1\}\{Y_G\}\}$, $\{W_2\} = \begin{Bmatrix} \{R_2\}\{Y_G\} \\ \{R_3\}\{Y_G\} \end{Bmatrix}$

Solving the first equation of Eq. (20), it yields:

$$\{P_1\} = [N_{1,1}]^{-1}\left(\{W_1\} - [N_{1,2}]\{P_2\}\right) \tag{21}$$

which provides the same result given by Eq. (18). Using this approach, which exploits the technique of partitioned matrices, the procedure developed in Section 2.1.1 for the analysis of the fixed arch can be applied also to the analysis of the arch on pinned supports, without any modification. This allows automation of the procedure and easy implementation in structural calculation software.

By entering k into Eq. (7), we get the ordinates of the vertices of the thrust line. To draw the line of thrust nearest to the geometric axis, Eq. (15) is used to build the vectors of abscissas and ordinates of the vertices of the thrust line.

2.2. Damaged arch

Due to unexpected external actions, the masonry arch may be damaged. Typical damage is the cracking at the intrados developed at the joint nearest to the point of application of a low magnitude point force, and the development of a second intrados crack, generally located at the impost farthest from the point force, for a point force of higher magnitude. These cracks can be considered as inner hinges, positioned at the boundary of the arch opposite the crack opening, which subdivide the arch into rigid portions linked only at the hinge points and, in the limit case, hinges are located at the intrados or extrados of these cracked joints. For this reason, if the magnitude of the point force is even higher, such as in the pictures shown in Fig. 3, a third extrados crack occurs in an intermediate position between the two extrados hinges, transforming the masonry arch to a statically determined structure (namely three-hinged), distinguished by a single line of thrust in equilibrium with the loads and the support reactions. It is worth noting that the condition necessary to develop a number of cracks less than 4 is the presence of deformable and cracking mortar joints between the blocks of the arch.

Another typical damage is that provided by the movement of supports, due to soil settlements or a very high thrust at the abutments. Even if it is ascertained, both empirically and numerically (Galassi et al., 2018, 2020a; Pippard and Ashby, 1939; Tralli et al., 2020), that at the onset of the movement of supports three cracks (i.e. hinges) instantly occur, in the case of vertically moving supports only two cracks are clearly opened (the intrados crack at the moving support joint and the extrados crack at a joint close to the fixed support) but only the former one is visible from the intrados while the second one is, generally, non-inspectable. The third crack, which occurs at the intrados of an intermediate joint, is always a microcrack at the onset of the movement, not fully opened and, therefore, it is negligible in the safety analysis. The effect of vertical movement of supports is shown in Fig. 4 referring to

Fig. 3. a) Arch damaged by the point force caused by the wooden beam supporting the roof at the right of the key; b) detail of the wooden beam causing the damage.

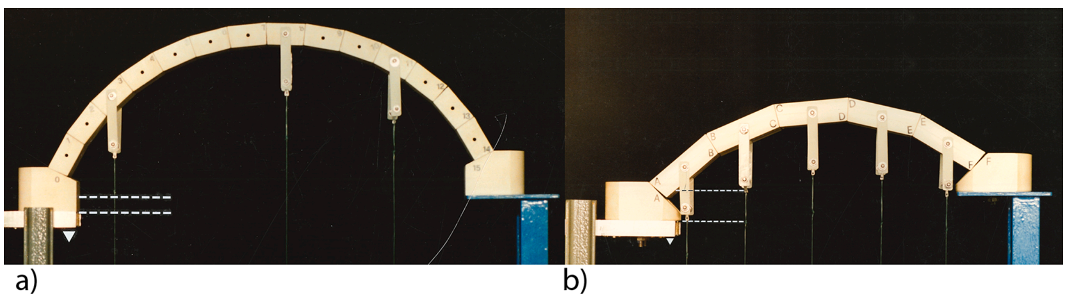

Fig. 4. a) Arch models subject to the downward movement of the left support: experimental trial on 14- and 5-block arches conducted by the authors.

some laboratory tests carried out by the authors (Galassi et al., 2018). Tests were carried out on scaled-down arch models made of PVC blocks to reduce the number of variables inherent in the masonry material. Geometrical characteristics and loading conditions of the specimens are detailed in the numerical example section, where these arches are analyzed. Tests were performed on a specifically designed apparatus provided with a mechanical jack able to transmit both vertical and horizontal displacements to the left support of the arches. During the trial, the movement of the left support was slowly increased until collapse, but, in the present work, the configuration consistent with the onset of the movement is the one we are interested in.

The purpose of the procedure is assessing the safety of damaged arches, in their configuration slightly different from the design configuration, with one or two cracked joints. The presence of one or two cracks requires the line of thrust to pass through the hinge points at the cracked joints (Galassi and Tempesta, 2023).

2.2.1. *The hinged arch*

Let us analyze the continuous arch of Fig. 5a, subject to the discrete set of *n* gravitational loads F_1, F_2, F_3, …, F_n, applied to the centroids G_i identified on the geometric axis at the intersection with their action lines. Let us further consider the opening of one or two hinges, C_j ($j = 1{,}2$), at the intrados or extrados of the arch. In the case of a rigid-block arch hinges are identified at the joints between blocks. Let us denote by n_c the number of inner hinges ($1 \leq n_c \leq 2$). The thrust line is a polyline passing through the given hinges and through points P_i, vertically aligned with the centroids G_i. Note that the thrust line is cuspidate at the vertices P_i where the external loads are applied (Fig. 1b) and passes

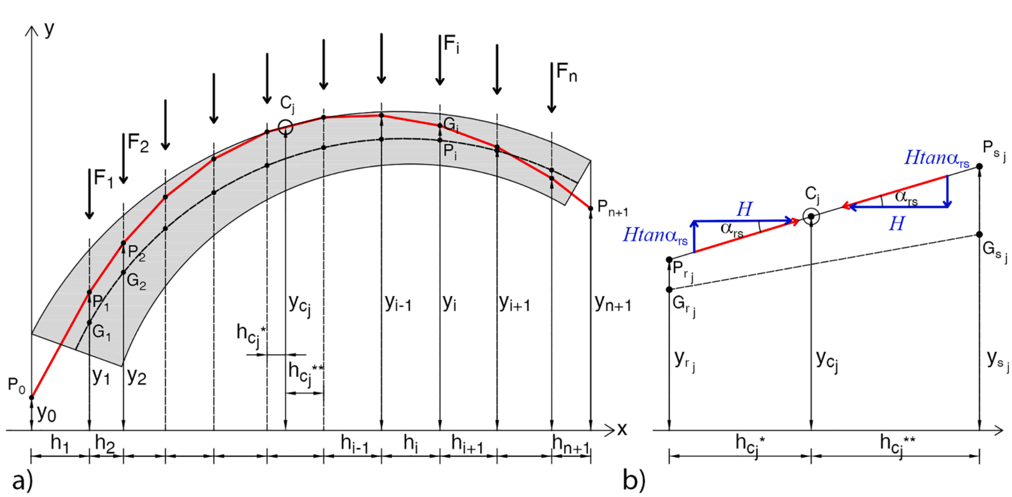

Fig. 5. a) Reference hinged arch; b) detail of the j-th ($j = 1{,}2$) hinge vertex C_j of the thrust line.

straight through the hinges (Fig. 5b). Accordingly, points P_i and C_j are denoted as *cusp vertices* and *hinge vertices*.

To compute the ordinates of the vertices of the line of thrust, the equilibrium equations of the hinge and the cusp vertices are formulated. The equilibrium equation between the vertical components of the inner forces and the external loads acting on the i-th cusp vertex $P_i \equiv (x_i, y_i)$ of the line of thrust is still expressed by Eq. (3) (Fig. 1b), which is also reported in Eq. (22) for the reader's clarity:

$$\left(\frac{-1}{h_i}\right)\cdot y_{i-1} + \left(\frac{h_i + h_{i+1}}{h_i \cdot h_{i+1}}\right)\cdot y_i + \left(\frac{-1}{h_{i+1}}\right)\cdot y_{i+1} = \frac{F_i}{H} \tag{22}$$

In addition, the equilibrium equation between the vertical components of the inner forces acting on the j-th hinge vertex $C_j \equiv (x_{C_j}, y_{C_j})$ of the line of thrust, with $1 \le j \le 2$, located between the cusp vertex P_{r_j} and P_{s_j}, is given in Eq. (23) (Fig. 5b):

$$\left(\frac{-1}{h_{c_j^*}}\right)\cdot y_{r_j} + \left(\frac{h_{c_j^*} + h_{c_j^{**}}}{h_{c_j^*} \cdot h_{c_j^{**}}}\right)\cdot y_{C_j} + \left(\frac{-1}{h_{c_j^{**}}}\right)\cdot y_{s_j} = 0 \tag{23}$$

Collecting the equilibrium equations of all vertices of the line of thrust, we get the system of $n + n_c$ linear equations in $n + 3$ unknowns in Eq. (24):

$$\begin{cases} \left(\frac{-1}{h_1}\right)\cdot y_0 + \left(\frac{h_1 + h_2}{h_1 \cdot h_2}\right)\cdot y_1 + \left(\frac{-1}{h_2}\right)\cdot y_2 = \frac{F_1}{H} \\ \left(\frac{-1}{h_2}\right)\cdot y_1 + \left(\frac{h_2 + h_3}{h_2 \cdot h_3}\right)\cdot y_2 + \left(\frac{-1}{h_3}\right)\cdot y_3 = \frac{F_2}{H} \\ \cdots\cdots\cdots\cdots\cdots\cdots\cdots\cdots \\ \left(\frac{-1}{h_i}\right)\cdot y_{i-1} + \left(\frac{h_i + h_{i+1}}{h_i \cdot h_{i+1}}\right)\cdot y_i + \left(\frac{-1}{h_{i+1}}\right)\cdot y_{i+1} = \frac{F_i}{H} \\ \cdots\cdots\cdots\cdots\cdots\cdots\cdots\cdots \\ \left(\frac{-1}{h_{r_j}}\right)\cdot y_{r_j-1} - \left(\frac{1}{h_{c_j^*}}\right)\cdot y_{C_j} + \left(\frac{h_{r_j} + h_{c_j^*}}{h_{r_j} \cdot h_{c_j^*}}\right)\cdot y_{r_j} = \frac{F_{r_j}}{H} \\ \left(\frac{-1}{h_{c_j^*}}\right)\cdot y_{r_j} + \left(\frac{h_{c_j^*} + h_{c_j^{**}}}{h_{c_j^*} \cdot h_{c_j^{**}}}\right)\cdot y_{C_j} + \left(\frac{-1}{h_{c_j^{**}}}\right)\cdot y_{s_j} = 0 \\ \left(\frac{h_{c_j^{**}} + h_{s_j+1}}{h_{c_j^{**}} \cdot h_{s_j+1}}\right)\cdot y_{s_j} - \left(\frac{1}{h_{c_j^{**}}}\right)\cdot y_{C_j} + \left(\frac{-1}{h_{s_j+1}}\right)\cdot y_{s_j+1} = \frac{F_{s_j}}{H} \\ \cdots\cdots\cdots\cdots\cdots\cdots\cdots\cdots \\ \left(\frac{-1}{h_n}\right)\cdot y_{n-1} + \left(\frac{h_n + h_{n+1}}{h_n \cdot h_{n+1}}\right)\cdot y_n + \left(\frac{-1}{h_{n+1}}\right)\cdot y_{n+1} = \frac{F_n}{H} \end{cases} \tag{24}$$

Note that the system of Eq. (24) is the extension of the system of Eq. (4) in order to consider also the hinge vertices.

In the system of Eq. (24) the unknowns to be calculated are the thrust H and the y_i ordinates of the $n + 2$ cusp vertices P_i of the line of thrust, including the first, P_0, and the last, P_{n+1}. However, the restriction that the line of thrust pass through one or two hinges reduces the indeterminacy of the static problem by one or two degrees.

To solve the problem, the system of Eq. (24) is rearranged by placing the equation(s) of the hinge vertex(ices) in the last row(s) and the three parameters that are isolated within the system of Eq. (24) are chosen as a function of the number n_c of hinges. The solution procedures for the one- and the two-hinged arch are given in Appendix A and Appendix B, respectively.

2.3. Implementation of horizontal loads

In this section the numerical procedure for identifying the thrust line nearest to the geometric axis of an arch is extended to also consider a system of horizontal forces proportional to gravitational loads. In this way, the procedure allows in-plane statically equivalent seismic analysis to be performed. For clarity, we refer to the discrete arch of Fig. 6a.

Since the numerical procedure works only for vertical loads, horizontal forces cannot be included in the arch model.

To get around this drawback, the effect of these horizontal actions is taken into account by exploiting the analogy between the structure in its actual position, subject to the combined actions of gravitational loads and horizontal forces, and the same structure, theoretically tilted by the angle corresponding to the direction of the resultant vectors, subjected to these loads, arranged vertically. Let us refer to the discrete arch of Fig. 6. Fig. 6a shows the arch at its actual position and the combined action of the gravitational load F_i and the horizontal force V_i applied to the centroid of each element *i*. Denoted as λ the seismic factor, the horizontal force caused by the earthquake is given by Eq. (25):

$$V_i = \lambda F_i \tag{25}$$

Exploiting the above analogy, the arch is tilted by the angle α that corresponds to the direction of the resultant vectors R_i (Fig. 6b) and the angle is calculated through Eq. (26):

$$\alpha = \arctan(\lambda) \tag{26}$$

Each element of the inclined structure is subject to the action of a fictitious vertical force R_i, the magnitude of which, equal to that of the

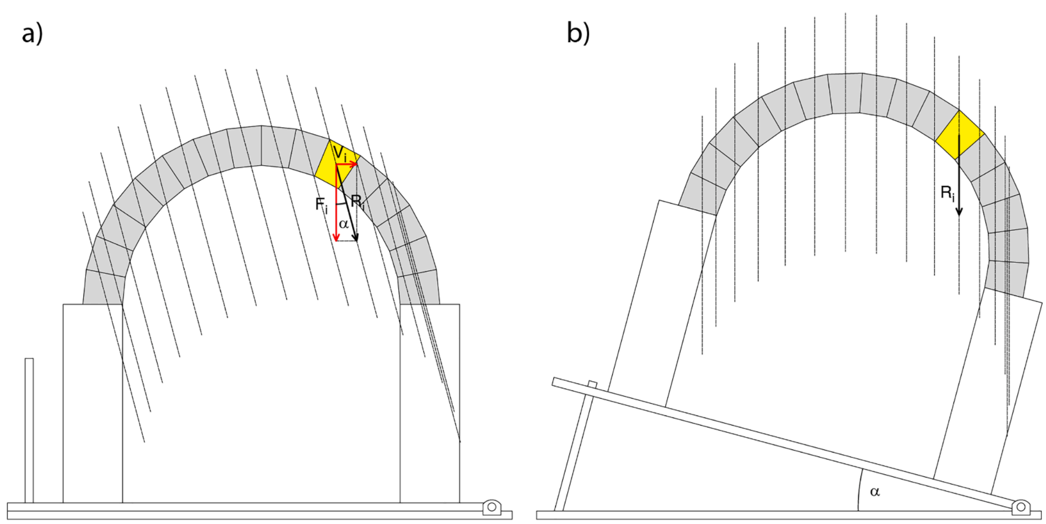

Fig. 6. Analogy between a) the actual arch subject to the combined action of gravitational loads and horizontal forces and b) the arch rotated at the angle α of the direction of the resultant vectors.

resultant vector of the gravitational load and the horizontal force, is calculated by Eq. (27):

$$R_i = \frac{F_i}{\cos(\alpha)} \tag{27}$$

Note that the seismic factor λ, which corresponds to the tangent of the tilt angle α, is also given by the ratio of the horizontal to vertical loads:

$$\lambda = \tan(\alpha) = \frac{V_i}{F_i} \tag{28}$$

To identify the line of thrust nearest to the geometric axis of an arch subject to the combined actions of gravitational loads and horizontal seismic forces, the procedure runs the following steps:

- for a given seismic factor λ, the angle α is calculated using Eq. (26);
- the vertical fictitious forces R_i applied to the centroids G_i are calculated using Eq. (27) and vector $\{T_1\}$ is built using Eq. (5);
- the arch is tilted by the angle α;
- the thrust line nearest to the geometric axis is identified by analyzing the tilted structure.

Since no one has pointed this out before, the authors wish to emphasize that Eqs. (25) to (28) prove that the tilt test, which is usually performed to simulate the action of an earthquake on a structure placed on the inclined platform of the trial, provides only qualitatively the seismic response but does not predict the seismic factor correctly, underestimating the seismic action which, instead, causes the collapse in advance. As highlighted by Eq. (27), the bug is that the vertical loads preserve constant during the test.

3. Safety assessment

According to Heyman's theory, identifying a line of thrust within the arch profile ensures the safety of the arch, but it does not measure its actual degree of safety, even if it is calculated as the nearest to the geometric axis. Furthermore, the line of thrust nearest to the geometric axis, provided by the analysis, may also be not entirely contained in the profile of the arch. This occurrence does not necessarily imply that the arch is not safe. Actually, this thrust line is only one of the ∞^3 funicular polygons for the assigned loads. It can be moved up or down to check whether it fits within the profile of the arch. This vertical movement allows one exploring the entire set of ∞^1 funicular polygons parallel to that identified by the procedure. In this perspective, we propose a method for computing the degree of safety of a masonry arch based on the identification of a region, that we denote as "domain of safety", which contains the set of ∞^1 funicular polygons, parallel to that provided by the procedure, within the profile of the arch (Fig. 7). Each

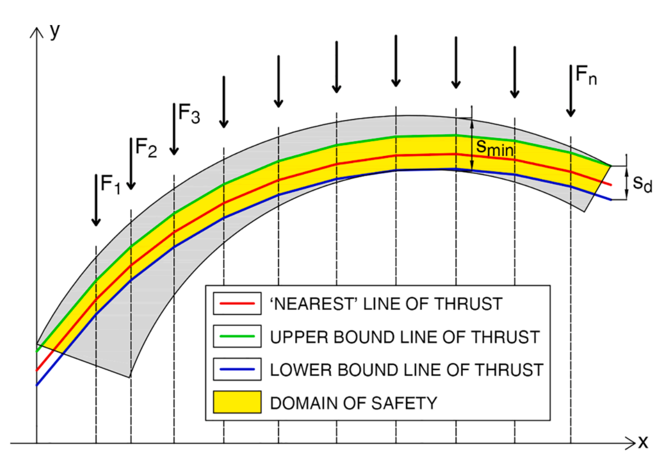

Fig. 7. Domain of safety.

funicular polygon of this set represents different equilibrium conditions. The lower and upper bounds of this region are marked by the line of thrust, parallel to that identified by the computation, tangent to the intrados and extrados, respectively, and entirely within the profile of the arch.

The degree of safety (referred to by the acronym "dos" in Eq. (29) based on this domain is calculated as follows:

$$\mathrm{dos} = \frac{S_d}{S_{min}} 0 \leq \mathrm{dos} \leq 1 \tag{29}$$

where s_d is the vertical thickness of the domain and s_{min} the minimum vertical thickness of the arch, measured in correspondence to the action lines of loads.

According to Eq. (29), the degree of safety of safe arches is a coefficient comprised in the interval [0,1]. The degree of safety equal to 1 indicates the safest arch since the thickness of the domain and the thickness of the arch are equal. This happens only in the case of an inverted catenary-shaped arch (Tempesta and Galassi, 2019). In contrast, the degree of safety equal to 0 indicates the least-safe arch because the thickness of the domain is zero. This occurs when there is only one thrust line within the arch profile. Negative values, instead, indicate unsafe arches.

To assess the degree of safety of an arch subject to horizontal actions defined on the basis of an assigned seismic factor λ, Eq. (29) can still be applied. However, if the purpose of the analysis is to evaluate the seismic capacity of an arch, it is necessary to calculate the limit seismic factor λ_{lim}. In the context of limit analysis, the limit seismic factor is that which activates the collapse mechanism. Instead, exploiting the procedure proposed here, the limit seismic factor is the one that makes the thickness of the domain null:

$$\lambda = \lambda_{lim} \rightarrow \alpha = \alpha_{max} \ : s_d = 0 \tag{30}$$

To calculate the limit seismic factor λ_{lim}, it is necessary to iteratively perform the four steps given at the end of the previous section for trial values of the angle α of the arch inclination. To this aim, it is worth noting that since the seismic factor varies in the range [0,1], the trial values of α accordingly vary in the range $\left[0, \frac{\pi}{2}\right]$. By applying the bisection method in this range, the limit seismic factor and the corresponding angle of inclination of the structure are quickly obtained. The iterative analysis is stopped when the thickness of the domain is zero.

It is worth noting that this procedure for assessing the degree of safety, based on a geometric approach, applies only to undamaged arches. In the case of damaged arches, the line of thrust, being required to pass through the hinges, cannot be shifted vertically within the arch profile and, as a result, the domain of safety cannot be identified, because it is reduced to a region of zero thickness. Therefore, for damaged arches, if this zero-thickness region is within their profile, the method allows one to assess the equilibrium condition but does not provide the degree of safety.

4. Numerical examples

The following examples refer to arches made of rigid blocks arranged along radial joints.

4.1. Symmetric arch subject to incremental point forces

Let us investigate the behaviour of the masonry arch shown in Fig. 8. It is a symmetric segmental arch, composed of 24 elements, it covers a span of 600 cm with an angle of embrace of 120° and a thickness of 50 cm; as a result, the rise is 173.2 cm. The unit weight of masonry is assumed to be 18 kN/m^3.

Let us consider the case of two additional point forces, applied symmetrically to one-third of the span and analyze the behaviour of the

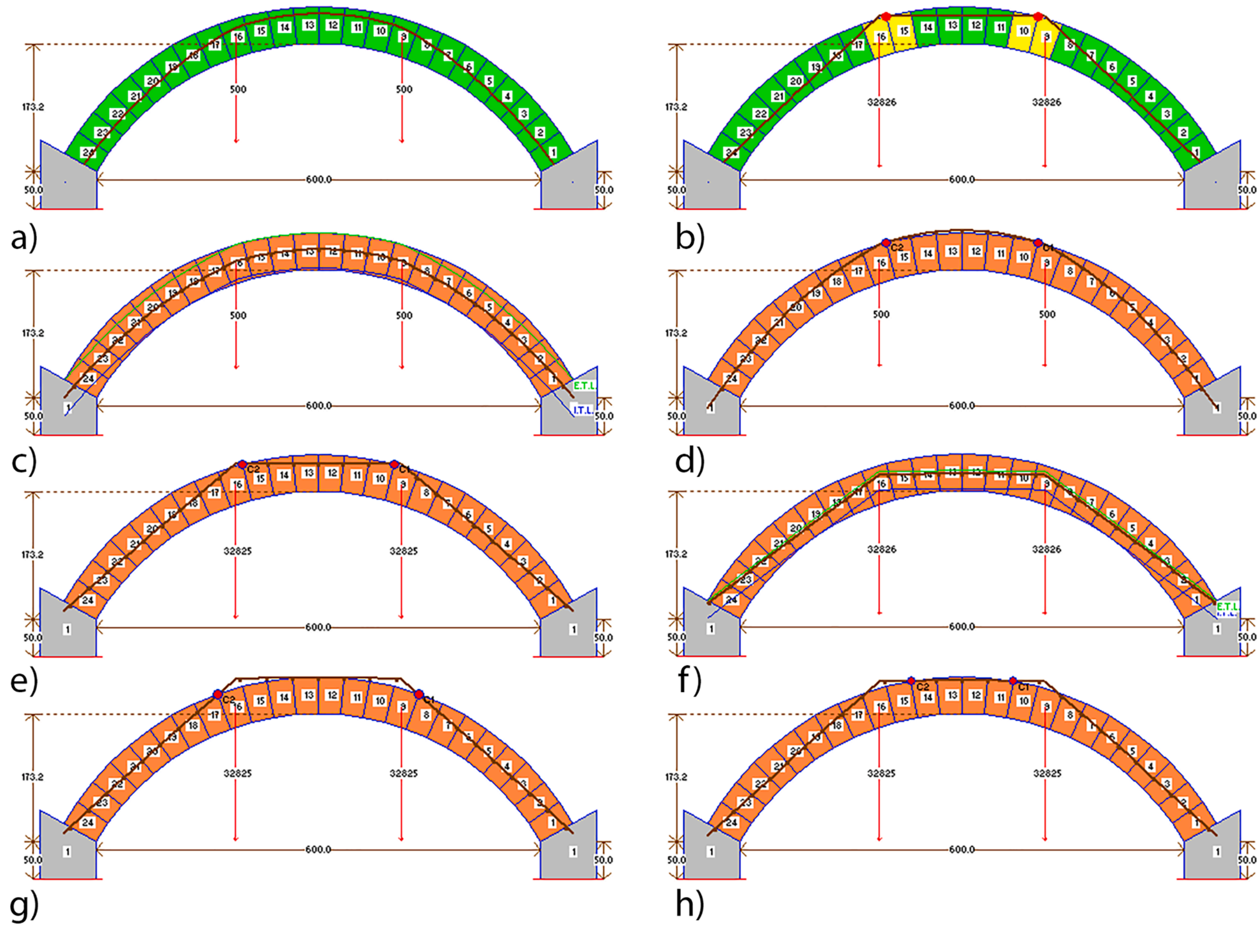

Fig. 8. Symmetric arch subject to incremental point forces. Thrust line provided by incremental analysis a) for the low magnitude point forces and b) for the value that causes the hinges to occur; c) thrust line nearest to the geometric axis of the arch in its actual undamaged configuration for low magnitude point forces and d) forced through the hinges that are not yet developed for this load level; e) thrust line nearest to the geometric axis of the arch forced through the hinges that develop for the load achieved in the incremental analysis and f) without any conditioning. In g) and h) the thrust line nearest to the geometric axis of the arch forced to pass through hinges displaced in the joints before and after those where they actually develop, respectively.

arch for different values of their magnitude. For this purpose, both the classic incremental analysis and the proposed procedure are used, and results are compared.

Fig. 8a shows that the shape of the thrust line, provided by the incremental analysis (Pugi and Galassi, 2013), is not much affected by the point forces when their magnitude is rather low, and that the arch is in equilibrium without developing any hinges. As the point forces increase, the shape of the thrust line provided by the incremental analysis changes and, for the value which causes the hinges to occur at the extrados of the joints nearest to the lines of action of the loads, takes on the trilinear shape shown in Fig. 8b. The shape of the thrust line no longer changes even if these point forces are increased to an infinite magnitude. Therefore, under the assumption of infinite strength of masonry, incremental analysis provides a theoretical infinite degree of safety shown by the thrust line of Fig. 8b that does not develop any collapse mechanism because it is entirely contained within the profile of the arch even if passes through the two hinges.

The behaviour of the arch, for the same load levels taken as a reference in the incremental analysis, is also investigated using the procedure proposed here. For low magnitude loads such as those in Fig. 8a, the thrust line nearest to the geometric axis of the arch is entirely contained within the profile of the arch and provides the very high degree of safety of 0.96 and the domain of safety is shown in Fig. 8c. An experiment was made, forcing the thrust line to pass through the extrados hinges shown in Fig. 8b. What you get is a thrust line indicating a nonequilibrium condition between inner forces and external loads (Fig. 8d), as it lies outside the arch profile at the crown. The result is that it is not possible to force the thrust line to pass through the assigned hinges because they are not developed for that load level. There must be a consistent relationship between causes (point forces) and effects (hinges developed by the forces) and the hinges cannot be assigned to the arch only merely as simple points through which the thrust line must pass.

For the same load level such as in Fig. 8b, which causes the hinges to develop, hinges are assigned to the joints indicated by the incremental analysis and the two-hinged arch is analyzed by looking for the thrust line nearest to the geometric axis obliged to pass through the hinges. What you get is a trilinear thrust line consistent with that provided by the incremental analysis, entirely within the profile of the arch (Fig. 8e). For the same load level, the analysis is rerun by assuming that the arch is undamaged (Fig. 8f). What is achieved is an even safer equilibrium condition, shown by a trilinear thrust line entirely contained in the profile of the arch that touches neither the intrados nor the extrados of the arch. It is concluded that the thrust line in equilibrium with the loads provided by the incremental analysis is not the only one possible nor that the degree of safety is infinite. Indeed, the domain of safety shown in Fig. 8f provides the degree of safety of 0.49, which still indicates high safety.

Also for this load level, the experiment to investigate the "role of hinges" in the equilibrium condition of the arch was made. The thrust line forced to pass through hinges displaced at the previous and next joints was determined (Fig. 8g and Fig. 8h). The obtained thrust line

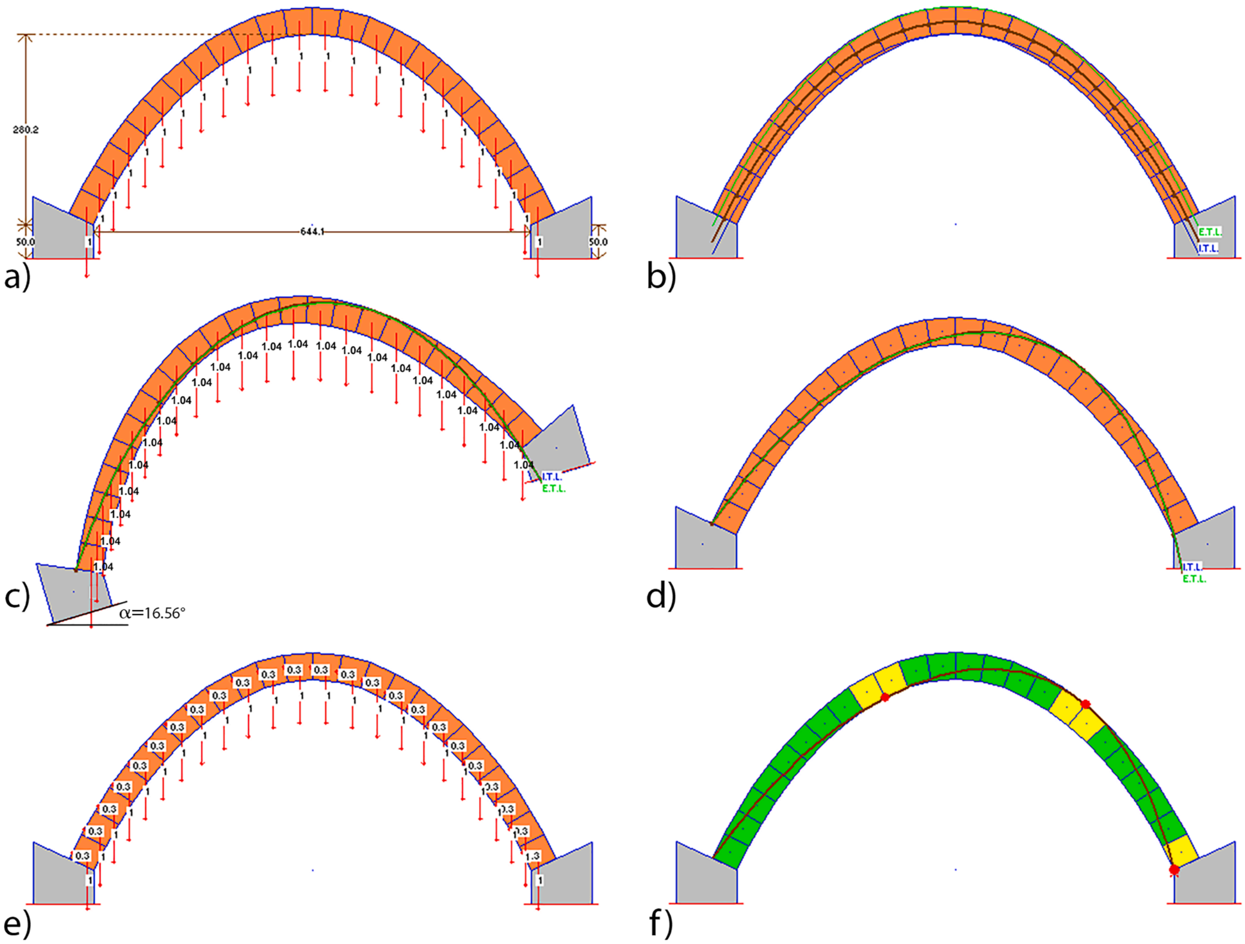

Fig. 9. a) Inverted catenary-shaped arch; b) thrust line and domain of safety for self-weight loads; c) thrust line for leftward horizontal forces provided by the procedure by tilting the platform counterclockwise without directly inserting them into the arch model and d) shown in the arch in its actual position; e) thrust line provided by limit analysis by inserting horizontal forces proportional to the gravitational loads and f) collapse mechanism.

indicates nonequilibrium, because it is not entirely within the profile of the arch. The result is that hinges cannot be placed randomly along the arch profile because, as mentioned above, there must be a consistent relationship between cause and effect.

4.2. Inverted catenary-shaped arch subject to horizontal loads

Let us consider the discrete inverted catenary-shaped arch analyzed by Tempesta and Galassi (2019) shown in Fig. 9a. It is composed of 24 elements and covers a span of 644.1 cm with an angle of embrace of 130.9°, while the rise and the constant thickness are 280.2 cm and 40 cm, respectively. In (Tempesta and Galassi, 2019) this arch was analyzed subject to self-weight loads to demonstrate the reliability of the procedure, which, indeed, provided a thrust line which overlapped almost perfectly with the geometric axis of the arch and a degree of safety of 1, indicating the highest safety level (Fig. 9b).

In this section, the arch is analyzed again to assess the effect of horizontal forces caused by an earthquake and compute the limit seismic factor. Unit self-weight loads are considered for the analysis because the shape of the thrust line is not affected by the magnitude of the loads if they are scaled by the same factor. In Fig. 9c and Fig. 9d the thrust line nearest to the geometric axis of the arch subject to leftward horizontal loads, proportional to the vertical ones, is shown. To simulate the action of these horizontal loads the platform on which the arch rests has been tilted counterclockwise, and the "virtual" vertical forces that capture the combined action of the gravitational loads and horizontal forces have been computed using Eq. (26). The angle at which the thickness of the domain becomes zero is calculated to be 16.56°. At this value, the degree of safety compulsorily becomes zero and the procedure finds the limit seismic factor $\lambda_{\mathrm{lim}} = 0.297$.

For comparison purposes, the analysis was also performed exploiting limit analysis (Fig. 9e) (Galassi et al., 2020b) which provided a seismic factor of 0.326 and the thrust line is shown in Fig. 9f.

By comparing the results provided by these two different approaches, it is worth noting that:

1) the limit condition from which the limit seismic factor is drawn is provided by zeroing the domain in the proposed procedure, while it is provided by the onset of the collapse mechanism exploiting limit analysis. Accordingly, the collapse mechanism provided by limit analysis is the four-hinge mechanism with hinges at the intrados of the right abutment, the extrados of the right haunch, the intrados of the left haunch and the extrados of the left abutment;
2) the limit condition of equilibrium is attained when the thrust line touches the intrados and the extrados of the arch in correspondence to four different joints where hinges open in limit analysis, while, exploiting our method, it is attained when the thrust line simultaneously touches both the intrados and extrados at a number of points usually less than four (three points in the case at hand). For this reason, the limit seismic factor provided by limit analysis is slightly higher than that provided by our method, which is consequently more conservative.

4.3. Arch on pinned supports

The effect of the downward movement of the left support on the 5-block arch model investigated in (Galassi et al., 2018) is shown in Fig. 4b. In this figure, where the displacement has already reached a high value, only the two cracks at the abutments are clearly visible, while the intermediate one is not noticeable. At the onset of the support movement, these cracks are even narrower and the geometry differs slightly from the original one. Based on this premise, using the proposed method the analysis can be performed by considering the case of an arch on pinned supports and its original geometry.

The arch is a reduced-scale model, made of PVC (14 kN/m^3), covering a span of 42.4 cm with an angle of embrace of 90°, has a thickness of 3 cm and a rise of 8.4 cm. Additional point forces are applied to the centroids of the blocks: 10 N to the first block on the left, 3 N to the second one, 5 N to the third and the fourth block, and 12 N to the last block on the right.

The thrust line nearest to the geometric axis of the arch obliged passing through the pinned supports is shown in Fig. 10a. What you get, is a thrust line equal to the one that you get due to a very small downward movement of the left support, which causes three hinges to open, but the intermediate one is not visible because there is a microcrack in that joint. For comparison purposes, Fig. 10b also shows the thrust line caused by the movement of the support and obtained using the numerical approach developed by Galassi et al. (2018). It follows that this procedure can be a useful tool to predict the causes of the visible damage on the arch and assess the safety of the damaged arch.

4.4. Arch damaged to inner joints

In Fig. 4a the 14-block arch model tested by the authors subject to the downward movement of the left support is shown. It is a reduced-scale arch model, made of PVC (14 kN/m^3), covering a span of 53.5 cm with an angle of embrace of 126°, has a thickness of 3 cm and a rise of 16.4 cm. Additional point forces are applied to the centroids of the blocks: 9 N to the third block on the left, 6 N to the seventh one, and 9 N to the eleventh block. During the trial, at the onset of the movement damage occurred at the inner joint 4, where the hinge opened at the extrados, and 14, where the hinge opened at the intrados, and at the joint at the left abutment, where the hinge opened at the extrados.

Also in this case study, the proposed method can be used to predict the causes of such a damage by considering the case of a two-hinged arch and its original geometry. For this purpose, by assigning the position of the inner hinges at joints 4 and 14, what you get is a thrust line (Fig. 11a) equal to the one that you get due to a very small downward movement of the left support (Fig. 11b) and obtained using the numerical approach developed by Galassi et al. (2018). As a matter of fact, the thrust line passing through the inner hinges also touches the extrados of the joint at the left abutment, where the third hinge caused by the movement of the support is located.

As in the previous example, this procedure was used here to predict the causes of visible damage on the arch and assess the safety of the damaged arch.

4.5. Case study of a ruined archway in a barn

Let us examine the real case of the archway in the barn shown in Fig. 3. The arch, which supports the upper part of the stone wall of the barn, is clearly damaged. The arch is separated into portions held together at one point by inner cracks and, as a result, the current shape of the arch is very different from the original. In particular, two very wide cracks are clearly visible, one at the intrados to the right of the key and one at the extrados of the right haunch. A minor crack is also present at the extrados of the left haunch. From observation and in-site inspection, it is assumed that the damage is caused by the transfer to the arch of the roof load from the wooden beam that rests on the masonry present above it, to the right of the key. In authors' opinion, this point force increased the thrust of the arch at the abutments and the right support, which was weaker than the left one, spread apart. As a result, to accommodate to the displaced abutment, the arch cracked in three joints.

The arch, which is 12 cm thick and 25 cm deep, is analyzed here in its current deformed and cracked shape, obtained by horizontally shifting the right impost by 7 cm of the original round rampant arch covering a span of 180 cm. The right impost is inclined 22.50° to the horizontal and the left one is inclined 11.40° (resulting in an angle of embrace of 146.10°). For the analysis, a conventional assessment of the loads acting on the arch was preliminarily performed, which considers the weight of the stone wall, the load transmitted by the roof and that transmitted by the wooden beam resting on the wall, modelled by two point forces applied to the centroids of the 10th and 11th blocks on the right. The contact points of the cracked joints are assumed to be inner hinges through which the thrust line must pass. Hinges are assigned to the widest cracks, namely the one at the key and the one at the right haunch, and the obtained two-hinged arch is analyzed using the proposed procedure. The thrust line nearest to the geometric axis obliged passing through the assigned hinges is located everywhere within the profile of the arch, except for the first block to the left, and touches the intrados point of the left haunch, thus highlighting the propensity of the structure to open the third crack precisely at this joint where, in fact, the minor crack is visible. On the other hand, it is worth noting that the tendency of the thrust line to exit the arch profile at the left impost, where an additional hinge could open, is prevented by the presence of the stone wall above the arch, modelled only as a load and neglecting that it also acts as a constraint.

The obtained thrust line is coherent with the deformed shape of the arch and the position of the cracks and highlights the new equilibrium condition of the arch as a result of the movement of the right support (Fig. 12). It is concluded that the procedure can be used to assess the safety and interpret the causes of even a very damaged arch in its actual deformed and cracked configuration.

5. Conclusions

The procedure proposed in this paper is an extension of that developed in a previous paper by the authors. The original procedure was formulated to calculate the thrust line nearest to the geometric axis of an arch and to evaluate, based on this, the safety level. However, it was

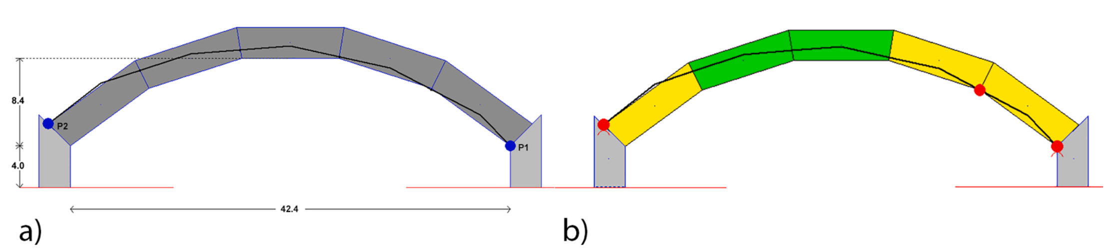

Fig. 10. 5-block arch model: a) thrust line nearest to the geometric axis obliged passing through the pinned supports; b) thrust line caused by the downward movement of the left support.

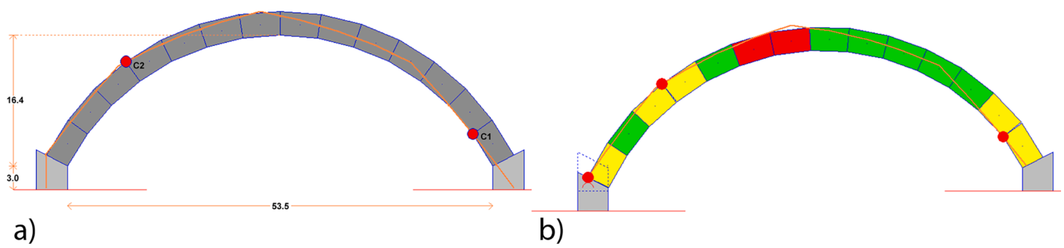

Fig. 11. 14-block arch model: a) thrust line nearest to the geometric axis obliged passing through the inner hinges; b) thrust line caused by the downward movement of the left support.

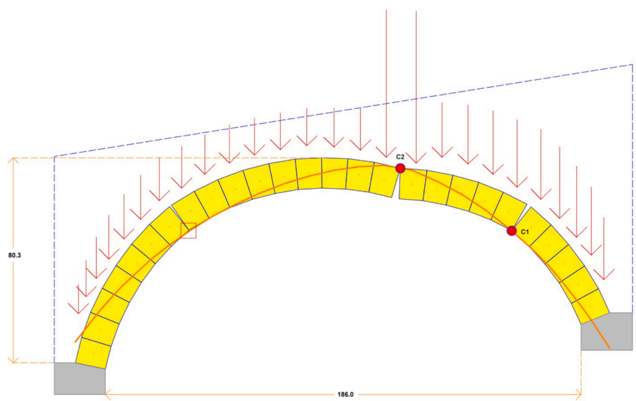

Fig. 12. Interpretation of the deformed configuration and position of the cracks in the archway of a barn.

limited to the analysis of arches fixed to their supports and subject only to vertical loads. The revisited procedure also makes it possible to assess safety against horizontal actions proportional to the gravitational loads, such as those caused by an earthquake, without including these horizontal forces directly in the structure model. Furthermore, the procedure is extended to also identify the thrust line nearest to the geometric axis obliged to pass through one or two predetermined points. With this extension, arches on pinned supports and one- or two-hinged arches can also be analyzed. Inner hinges incorporate damage caused by unexpected actions such as the movement of supports caused by soil settlement or increased vertical or horizontal loads. Similarly, arches on pinned supports can be considered as arches constructed with geometric defects and placed on imperfect joints. Following this reasoning, the extended procedure allows damaged arches to be analyzed as well, which is something new in the literature. Both arches at the beginning of the damage in their original geometric configuration and very damaged arches in a "deformed" and cracked configuration can be analyzed with this procedure. To handle all load and constraint cases and the occurrence of damage with a single numerical procedure, the extended procedure is completely reformulated by exploiting the technique of partitioned matrices. Thus, this procedure is well suited to be automated and to be easily developed in structural calculation software.

A verification tool is also proposed, that consists of identifying the domain of admissible lines of thrust (namely a domain of safety), that provides a factor of safety. The safety factor can always be obtained with this tool, even for arches subject to standard operational loads, whereas limit analysis methods calculate the factor of safety only for arches at collapse. When considering the ultimate limit state and an additional incremental load, the method presented here provides a lower factor of safety than that provided by the limit analysis (Section 4.2); therefore, this method is more conservative. In addition, there are particular structures subjected to additional increasing loads for which limit analysis, under the assumption of infinite strength of the material, cannot find the safety factor either because of the peculiar shape of these structures and external constraints, such as the double fixed arch-beam or lintel (where no alternating combination of four hinges can trigger a compatible collapse mechanism) or because of the peculiar condition of an additional load such as that in the example given in Section 4.1 (arch subject to incremental point forces). The verification tool proposed here succeeds in finding a safety factor for these structures as well.

The robustness and reliability of the procedure are demonstrated by analyzing numerical examples of properly designed arches as well as scale models of arches damaged by the movement of supports by the authors and a real archway in a barn damaged by the point force transferred from the roof support beam. Hence, the procedure proposed can be used not only to assess the safety level of an undamaged arch subject to gravitational and horizontal forces but also to predict the causes of visible damage on the arch.

CRediT authorship contribution statement

Stefano Galassi: Writing – review & editing, Writing – original draft, Validation, Supervision, Software, Methodology, Investigation, Formal analysis, Data curation, Conceptualization. **Giacomo Tempesta:** Writing – review & editing, Writing – original draft, Validation, Supervision, Methodology, Investigation, Formal analysis, Data curation, Conceptualization.

Declaration of Competing Interest

The authors declare that they have no known competing financial interests or personal relationships that could have appeared to influence the work reported in this paper.

Data availability

No data was used for the research described in the article.

Appendix 1

Appendix A. Solution for the one-hinged arch

For the one-hinged arch ($j = 1$, $n_c = 1$), the three redundant parameters are $k = 1/H$ and y_0, which are unknowns, and y_{C_1}, which is given, and the system in Eq. (24) takes the matrix form of Eq. (A.1):

$$[\mathrm{D}]\{\mathrm{Y}\} = \{\mathrm{T}_1\}\cdot \mathrm{k} + \{\mathrm{T}_2\}\cdot \mathrm{y}_0 + \{\mathrm{T}_3\}\cdot \mathrm{y}_{\mathrm{C}_1} \tag{A1}$$

where:

$$\mathrm{D} = \begin{bmatrix} \left(\frac{h_1+h_2}{h_1\cdot h_2}\right) & \left(\frac{-1}{h_2}\right) & 0 & 0 & 0 & 0 & 0 & 0 & 0 & 0 \\ \left(\frac{-1}{h_2}\right) & \left(\frac{h_2+h_3}{h_2\cdot h_3}\right) & \left(\frac{-1}{h_3}\right) & 0 & 0 & 0 & 0 & 0 & 0 & 0 \\ \cdots & \cdots & \cdots & \cdots & \cdots & \cdots & \cdots & \cdots & \cdots & \cdots \\ 0 & 0 & \left(\frac{-1}{h_i}\right) & \left(\frac{h_i+h_{i+1}}{h_i\cdot h_{i+1}}\right) & \left(\frac{-1}{h_{i+1}}\right) & 0 & 0 & 0 & 0 & 0 \\ \cdots & \cdots & \cdots & \cdots & \cdots & \cdots & \cdots & \cdots & \cdots & \cdots \\ 0 & 0 & 0 & 0 & \left(\frac{-1}{h_{r_1}}\right) & \left(\frac{h_{r_1}+h_{c_1^*}}{h_{r_1}\cdot h_{c_1^*}}\right) & 0 & 0 & 0 & 0 \\ 0 & 0 & 0 & 0 & 0 & 0 & \left(\frac{h_{c_1^{**}}+h_{s_1+1}}{h_{c_1^{**}}\cdot h_{s_1+1}}\right) & \left(\frac{-1}{h_{s_1+1}}\right) & 0 & 0 \\ \cdots & \cdots & \cdots & \cdots & \cdots & \cdots & \cdots & \cdots & \cdots & \cdots \\ 0 & 0 & 0 & 0 & 0 & 0 & 0 & \left(\frac{-1}{h_n}\right) & \left(\frac{h_n+h_{n+1}}{h_n\cdot h_{n+1}}\right) & \left(\frac{-1}{h_{n+1}}\right) \\ 0 & 0 & 0 & 0 & 0 & \left(\frac{-1}{h_{c_1^*}}\right) & \left(\frac{-1}{h_{c_1^{**}}}\right) & 0 & 0 & 0 \end{bmatrix},$$

$$\mathrm{Y} = \begin{Bmatrix} y_1 \\ y_2 \\ \cdots \\ y_i \\ \cdots \\ y_{r_1} \\ y_{s_1} \\ \cdots \\ y_n \\ y_{n+1} \end{Bmatrix}, \mathrm{T}_1 = \begin{Bmatrix} F_1 \\ F_2 \\ \cdots \\ F_i \\ \cdots \\ F_{r_1} \\ F_{s_1} \\ \cdots \\ F_n \\ 0 \end{Bmatrix}.\mathrm{T}_2 = \begin{Bmatrix} 1/h_1 \\ 0 \\ \cdots \\ 0 \\ \cdots \\ 0 \\ 0 \\ \cdots \\ 0 \\ 0 \end{Bmatrix}, \mathrm{T}_3 = \begin{Bmatrix} 0 \\ 0 \\ \cdots \\ 0 \\ \cdots \\ \frac{1}{h_{c_1^*}} \\ \frac{1}{h_{c_1^{**}}} \\ \cdots \\ 0 \\ -\left(\frac{h_{c_1^*}+h_{c_1^{**}}}{h_{c_1^*}\cdot h_{c_1^{**}}}\right) \end{Bmatrix} \tag{A2}$$

with:

- $[\mathrm{D}] \in \Re^{(n+1)\cdot(n+1)}$ the matrix of the coefficients of the unknowns which is partitioned in such a way as to highlight, in the last row (n + 1), the equilibrium condition of the hinge vertex and, in the last column (n + 1), the nonzero component related to the last vertex of the thrust line;
- $\{\mathrm{Y}\} \in \Re^{n+1}$ the vector collecting the ordinates of the cusp vertices of the line of thrust, i.e. the unknowns of the equilibrium problem;
- $\{\mathrm{T}_1\} \in \Re^{n+1}$ the vector partitioned to collect components for the loads F_i at the cusp vertices and null components expressing that there is no load at the hinge vertex;
- $\{\mathrm{T}_2\} \in \Re^{n+1}$ a vector whose only nonzero component is the coefficient $\frac{1}{h_1}$ of the unknown y_0;
- $\{\mathrm{T}_3\} \in \Re^{n+1}$ a vector whose only nonzero components are the coefficients of the ordinate y_{C_1} of the given hinge vertex.

The solution of Eq. (A.1) is given in Eq. (A.3):

$$\{\mathrm{Y}\} = \{\mathrm{R}_1\}\cdot \mathrm{k} + \{\mathrm{R}_2\}\cdot \mathrm{y}_0 + \{\mathrm{R}_3\}\cdot \mathrm{y}_{\mathrm{C}_1} \tag{A3}$$

with:

$$\{\mathrm{R}_1\} \in \Re^{n+1}, \{\mathrm{R}_2\} \in \Re^{n+1}, \{\mathrm{R}_3\} \in \Re^{n+1}$$

To identify the line of thrust nearest to the geometric axis that passes through the hinge vertex in the set of the ∞^{3-n_c} thrust lines ($n_c = 1$ in the case at hand), the function S is computed:

$$\mathrm{S} = \sum_{i=1}^{n+n_c} (\Delta y_i)^2 = \sum_{i=1}^{n+n_c} (y_i - y_{Gi})^2 \tag{A4}$$

In matrix form:

$$S = (\{Y\} - \{Y_G\})^2 = \left(\{R_1\} \cdot k + \{R_2\} \cdot y_0 + \{R_3\} \cdot y_{C_1} - \{Y_G\}\right)^2 \tag{A5}$$

It is worth noting that Eq. (A.3) is the same equation of Eq. (7) and Eq. (A.5) is the same equation of Eq. (9) where the unknown y_{n+1} is replaced by the given term y_{C_1}.

Function S is minimized by setting its partial derivatives, calculated with respect to the *3-n_c* redundant unknowns (n_c coefficients being assigned terms), equal to zero:

$$\begin{aligned} &\frac{\partial S}{\partial k}(k, y_0) = 0 \\ &\frac{\partial S}{\partial y_0}(k, y_0) = 0 \end{aligned} \tag{A6}$$

Eq. (A.6) leads to the following system of two linear equations:

$$\begin{cases} \{R_1\}^2 \cdot k + \{R_1\}\{R_2\} \cdot y_0 = \{R_1\}\left(\{Y_G\} - \{R_3\} \cdot y_{C_1}\right) \\ \{R_1\}\{R_2\} \cdot k + \{R_2\}^2 \cdot y_0 = \{R_2\}\left(\{Y_G\} - \{R_3\} \cdot y_{C_1}\right) \end{cases} \tag{A7}$$

i.e., in matrix form:

$$\begin{bmatrix} \{R_1\}^2 & \{R_1\}\{R_2\} \\ \{R_1\}\{R_2\} & \{R_2\}^2 \end{bmatrix} \cdot \begin{Bmatrix} k \\ y_0 \end{Bmatrix} = \begin{Bmatrix} \{R_1\}\left(\{Y_G\} - \{R_3\} \cdot y_{C_1}\right) \\ \{R_2\}\left(\{Y_G\} - \{R_3\} \cdot y_{C_1}\right) \end{Bmatrix} \tag{A8}$$

The same matrix equation (Eq. (A.8) is conveniently achieved following the approach discussed in the section 2.1.2, i.e. by taking Eq. (12) where the term y_{n+1} is replaced by y_{C_1} and by partitioning matrices and vectors to separate components related to the unknowns k and y_0 from components related to the prefixed term y_{C_1}, as indicated in Eq. (A.9):

$$\begin{bmatrix} \{R_1\}^2 & \{R_1\}\{R_2\} & \{R_1\}\{R_3\} \\ \{R_1\}\{R_2\} & \{R_2\}^2 & \{R_2\}\{R_3\} \\ \{R_1\}\{R_3\} & \{R_2\}\{R_3\} & \{R_3\}^2 \end{bmatrix} \cdot \begin{Bmatrix} k \\ y_0 \\ y_{C_1} \end{Bmatrix} = \begin{Bmatrix} \{R_1\}\{Y_G\} \\ \{R_2\}\{Y_G\} \\ \{R_3\}\{Y_G\} \end{Bmatrix} \tag{A9}$$

that is:

$$\begin{bmatrix} N_{1,1} & N_{1,2} \\ N_{2,1} & N_{2,2} \end{bmatrix} \cdot \begin{Bmatrix} P_1 \\ P_2 \end{Bmatrix} = \begin{Bmatrix} W_1 \\ W_2 \end{Bmatrix} \tag{A10}$$

where the submatrices of [N] are: $[N_{1,1}] = \begin{bmatrix} \{R_1\}^2 & \{R_1\}\{R_2\} \\ \{R_1\}\{R_2\} & \{R_2\}^2 \end{bmatrix}$, $[N_{1,2}] = \begin{bmatrix} \{R_1\}\{R_3\} \\ \{R_2\}\{R_3\} \end{bmatrix}$, $[N_{2,1}] = [\,\{R_1\}\{R_3\} \quad \{R_2\}\{R_3\}\,]$, $[N_{2,2}] = [\,\{R_3\}^2\,]$, the sub-vectors of $\{P\}$ are: $\{P_1\} = \begin{Bmatrix} k \\ y_0 \end{Bmatrix}$, $\{P_2\} = \{y_{C_1}\}$ and the sub-vectors of $\{W\}$ are: $\{W_1\} = \begin{Bmatrix} \{R_1\}\{Y_G\} \\ \{R_2\}\{Y_G\} \end{Bmatrix}$, $\{W_2\} = \{\{R_3\}\{Y_G\}\}$.

Solving the first equation of Eq. A.10, it yields:

$$\{P_1\} = [N_{1,1}]^{-1}\left(\{W_1\} - [N_{1,2}]\{P_2\}\right) \tag{A11}$$

which provides Eq. (A.8). It is worth noting that this equation is equal to Eq. (21), except for the size of the matrices and vectors which is of order 2.

The unknowns, k and y_0, components of sub-vector $\{P_1\}$, are obtained by solving Eq. A.11 (i.e. Eq. (A.8) and the ordinates of the vertices of the line of thrust are computed by entering these coefficients into Eq. (A.3).

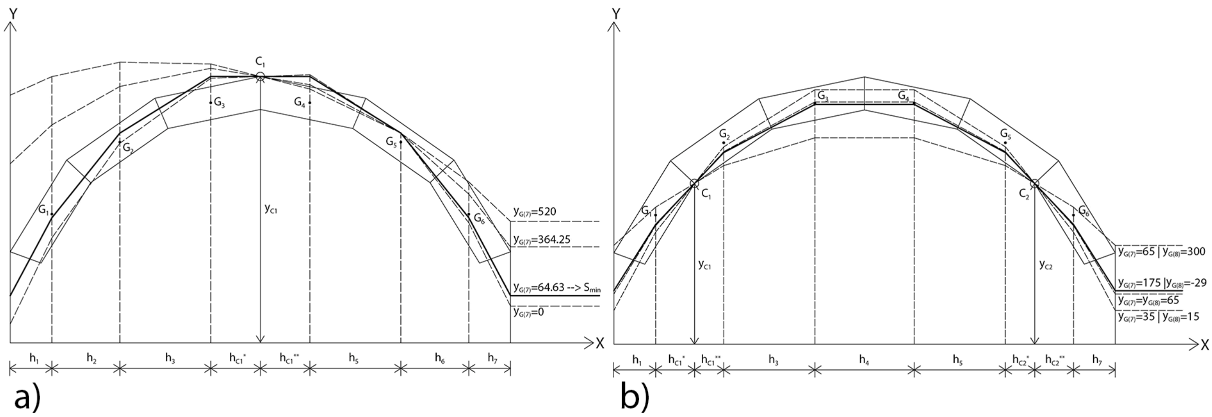

Fig. A1. Thrust lines passing through the hinges obtained for trial values of and (dashed polylines) and the one that is also nearest to the geometric axis (bold polylines): a) one-hinged arch; b) two-hinged arch.

However, it should be noted that Eq. A.11 does not provide a unique solution because it depends on the function S written in Eq. (A.5), which depends on the ordinate $y_{G(n+1)}$ of the fictitious centroid G_{n+1}. In fact, as shown in the reference six rigid-block arch of Fig. A1a, by setting for $y_{G(n+1)}$ different values, the full range of lines of thrust passing through the hinge and characterized by different distance from the geometric axis of the arch and different shape can be explored.

To find the line of thrust that passes through the hinge and nearest to the geometric axis, a trial-and-error procedure was devised, as follows. For trial values of $y_{G(n+1)} < y_{G(n)}$, the procedure iteratively:

- updates vector $\{Y_G\}$ and computes vector $\{W_1\} - [N_{1,2}]\{P_2\}$, accordingly;
- solves Eq. A.11 and finds the unknown $\{P_1\} = \begin{Bmatrix} k \\ y_0 \end{Bmatrix}$;
- computes the ordinates of the vertices of the line of thrust, by entering the current value of k and y_0 into Eq. (A.3);
- computes the squared distance function in Eq. (A.4) excluding the ordinate of the vertex P_{n+1} of the thrust line and of the fictitious centroid G_{n+1}, that is by solving the equation $S = \sum_{i=1}^{n} (\Delta y_i)^2 = \sum_{i=1}^{n} (y_i - y_{Gi})^2$ for the *n* points G_i and P_i.

The procedure stops when the value of $y_{G(n+1)}$ corresponds to the minimum of the function S and provides the two unknowns in Eq. A.11 and the ordinates of the vertices of the line of thrust.

Appendix B. Solution for the two-hinged arch

For the two-hinged arch ($j = 1$ to 2, $n_c = 2$), the three redundant parameters are $k = 1/H$, which is unknown, y_{C_1} and y_{C_2}, which are given, and the system in Eq. (24) takes the matrix form of Eq. (B.1):

$$[D]\{Y\} = \{T_1\}\cdot k + \{T_2\}\cdot y_{C_1} + \{T_3\}\cdot y_{C_2} \tag{B1}$$

where:

$$D = \begin{bmatrix}
\left(\frac{h_1+h_2}{h_1\cdot h_2}\right) & \left(\frac{-1}{h_2}\right) & 0 & 0 & 0 & 0 & 0 & 0 & 0 & 0 & \left(\frac{-1}{h_1}\right) \\
\left(\frac{-1}{h_2}\right) & \left(\frac{h_2+h_3}{h_2\cdot h_3}\right) & \left(\frac{-1}{h_3}\right) & 0 & 0 & 0 & 0 & 0 & 0 & 0 & 0 \\
\cdots & \cdots & \cdots & \cdots & \cdots & \cdots & \cdots & \cdots & \cdots & \cdots & \cdots \\
0 & 0 & \left(\frac{-1}{h_i}\right) & \left(\frac{h_i+h_{i+1}}{h_i\cdot h_{i+1}}\right) & \left(\frac{-1}{h_{i+1}}\right) & 0 & 0 & 0 & 0 & 0 & 0 \\
\cdots & \cdots & \cdots & \cdots & \cdots & \cdots & \cdots & \cdots & \cdots & \cdots & \cdots \\
0 & 0 & 0 & 0 & \left(\frac{-1}{h_{r_j}}\right) & \left(\frac{h_{r_j}+h_{c_j^*}}{h_{r_j}\cdot h_{c_j^*}}\right) & 0 & 0 & 0 & 0 & 0 \\
0 & 0 & 0 & 0 & 0 & 0 & \left(\frac{h_{c_j^{**}}+h_{s_j+1}}{h_{c_j^{**}}\cdot h_{s_j+1}}\right) & \left(\frac{-1}{h_{s_j+1}}\right) & 0 & 0 & 0 \\
\cdots & \cdots & \cdots & \cdots & \cdots & \cdots & \cdots & \cdots & \cdots & \cdots & \cdots \\
0 & 0 & 0 & 0 & 0 & 0 & 0 & \left(\frac{-1}{h_n}\right) & \left(\frac{h_n+h_{n+1}}{h_n\cdot h_{n+1}}\right) & \left(\frac{-1}{h_{n+1}}\right) & 0 \\
0 & 0 & 0 & 0 & 0 & \left(\frac{-1}{h_{c_1^*}}\right) & \left(\frac{-1}{h_{c_1^{**}}}\right) & 0 & 0 & 0 & 0 \\
0 & 0 & 0 & 0 & 0 & \left(\frac{-1}{h_{c_2^*}}\right) & \left(\frac{-1}{h_{c_2^{**}}}\right) & 0 & 0 & 0 & 0
\end{bmatrix},$$

$$Y=\begin{Bmatrix} y_1\\ y_2\\ \cdots\\ y_i\\ \cdots\\ y_{r_j}\\ y_{s_j}\\ \cdots\\ y_n\\ y_{n+1}\\ y_{n+2}\end{Bmatrix}, T_1=\begin{Bmatrix} F_1\\ F_2\\ \cdots\\ F_i\\ \cdots\\ F_{r_j}\\ F_{s_j}\\ \cdots\\ F_n\\ 0\\ 0\end{Bmatrix}. T_2=\begin{Bmatrix} 0\\ 0\\ \cdots\\ 0\\ \cdots\\ \frac{1}{h_{c_1^*}}\\ \frac{1}{h_{c_1^{**}}}\\ \cdots\\ 0\\ -\left(\frac{h_{c_1^*}+h_{c_1^{**}}}{h_{c_1^*}\cdot h_{c_1^{**}}}\right)\\ 0\end{Bmatrix}, T_3=\begin{Bmatrix} 0\\ 0\\ \cdots\\ 0\\ \cdots\\ \frac{1}{h_{c_2^*}}\\ \frac{1}{h_{c_2^{**}}}\\ \cdots\\ 0\\ 0\\ -\left(\frac{h_{c_2^*}+h_{c_2^{**}}}{h_{c_2^*}\cdot h_{c_2^{**}}}\right)\end{Bmatrix} \tag{B2}$$

with:

- $[D] \in \Re^{(n+2)\cdot(n+2)}$ the matrix of the coefficients of the unknowns which is partitioned in such a way as to highlight, in the last rows, $(n+1)$ and $(n+2)$, the equilibrium condition of the hinge vertices and, in the last columns, $(n+1)$ and $(n+2)$, the nonzero components related to the last and the first vertices of the thrust line, respectively;
- $\{Y\} \in \Re^{n+2}$ the vector collecting the ordinates of the cusp vertices of the line of thrust, i.e. the unknowns of the equilibrium problem;
- $\{T_1\} \in \Re^{n+2}$ the vector partitioned to collect components for the loads F_i at the cusp vertices and null components expressing that there is no load at the hinge vertices;
- $\{T_2\} \in \Re^{n+2}$ a vector whose only nonzero components are the coefficients of the ordinate y_{C_1} of the first hinge vertex.
- $\{T_3\} \in \Re^{n+2}$ a vector whose only nonzero components are the coefficients of the ordinate y_{C_2} of the second hinge vertex.

For reasons of matrix computation, the first and the last column of matrix [D] in Eq. (B.2) were switched so that the unknown y_0 was renamed as y_{n+2}.

The solution of Eq. (B.1) is given in Eq. (B.3):

$$\{Y\} = \{R_1\}\cdot k + \{R_2\}\cdot y_{C_1} + \{R_3\}\cdot y_{C_2} \tag{B3}$$

with:

$$\{R_1\} \in \Re^{n+2}, \{R_2\} \in \Re^{n+2}, \{R_3\} \in \Re^{n+2}$$

To identify the line of thrust nearest to the geometric axis that passes through the hinge vertices in the set of the ∞^{3-n_c} thrust lines ($n_c = 2$ in the case at hand), the function S is computed (Eq. (A.4). In matrix form, Eq. (A.4) becomes:

$$S = (\{Y\} - \{Y_G\})^2 = \left(\{R_1\}\cdot k + \{R_2\}\cdot y_{C_1} + \{R_3\}\cdot y_{C_2} - \{Y_G\}\right)^2 \tag{B4}$$

Note that Eq. (B.3) is the same equation of Eq. (7) and Eq. (B.4) is the same equation of Eq. (9) where the unknowns $y_0 = y_{n+2}$ and y_{n+1} are replaced by the given terms y_{C_1} and y_{C_2}, respectively.

Function S is minimized by setting its derivative, calculated with respect to the redundant unknown k, equal to zero (Eq. (16), leading to the linear equation that follows:

$$\{R_1\}^2\cdot k = \{R_1\}\left(\{Y_G\} - \{R_2\}\cdot y_{C_1} - \{R_3\}\cdot y_{C_2}\right) \tag{B5}$$

which provides the value of the unknown k:

$$k = \frac{\{R_1\}\left(\{Y_G\} - \{R_2\}\cdot y_{C_1} - \{R_3\}\cdot y_{C_2}\right)}{\{R_1\}^2} \tag{B6}$$

Exploiting the technique of partitioned matrices, already used in the previous sections, the same result is achieved by taking Eq. (12) where the terms y_0 and y_{n+1} are replaced by y_{C_1} and y_{C_2}, respectively, and by partitioning matrices and vectors to separate components related to the unknown k from components related to the prefixed terms y_{C_1} and y_{C_2}, as indicated in Eq. (B.7):

$$\begin{bmatrix} \{R_1\}^2 & \{R_1\}\{R_2\} & \{R_1\}\{R_3\} \\ \{R_1\}\{R_2\} & \{R_2\}^2 & \{R_2\}\{R_3\} \\ \{R_1\}\{R_3\} & \{R_2\}\{R_3\} & \{R_3\}^2 \end{bmatrix} \cdot \begin{Bmatrix} k \\ y_{C_1} \\ y_{C_2} \end{Bmatrix} = \begin{Bmatrix} \{R_1\}\{Y_G\} \\ \{R_2\}\{Y_G\} \\ \{R_3\}\{Y_G\} \end{Bmatrix} \tag{B7}$$

that is:

$$\begin{bmatrix} N_{1,1} & N_{1,2} \\ N_{2,1} & N_{2,2} \end{bmatrix} \cdot \begin{Bmatrix} P_1 \\ P_2 \end{Bmatrix} = \begin{Bmatrix} W_1 \\ W_2 \end{Bmatrix} \tag{B8}$$

where the submatrices of [N] are: $[N_{1,1}] = \left[\{R_1\}^2\right]$, $[N_{1,2}] = [\{R_1\}\{R_2\} \quad \{R_1\}\{R_3\}]$, $[N_{2,1}] = \begin{bmatrix} \{R_1\}\{R_2\} \\ \{R_1\}\{R_3\} \end{bmatrix}$, $[N_{2,2}] = \begin{bmatrix} \{R_2\}^2 & \{R_2\}\{R_3\} \\ \{R_2\}\{R_3\} & \{R_3\}^2 \end{bmatrix}$, the sub-vectors of $\{P\}$ are: $\{P_1\} = \{k\}$, $\{P_2\} = \begin{Bmatrix} y_{C_1} \\ y_{C_2} \end{Bmatrix}$ and the sub-vectors of $\{W\}$ are: $\{W_1\} = \{\{R_1\}\{Y_G\}\}$, $\{W_2\} = \begin{Bmatrix} \{R_2\}\{Y_G\} \\ \{R_3\}\{Y_G\} \end{Bmatrix}$

Solving the first equation of Eq. (B.8), it yields:

$$\{P_1\} = [N_{1,1}]^{-1}(\{W_1\} - [N_{1,2}]\{P_2\}) \tag{B9}$$

which provides the solution of Eq. (B.6). It is worth noting that this equation is equal to both Eq. (21) and Eq. A.11. The size of matrices and vectors in Eq. (B.9) is of order 1.

The ordinates of the vertices of the line of thrust are then calculated by entering k into Eq. (B.3).

Nevertheless, such as for the one-hinged arch, also in this case Eq. (B.9) does not provide a unique solution because it depends on the function S written in Eq. (B.4), which depends on the ordinate $y_{G(0)}$ of the fictitious centroid G_0 and the ordinate $y_{G(n+1)}$ of the fictitious centroid G_{n+1}. In fact, as shown in the reference six rigid-block arch of Fig. A.1b, by setting for $y_{G(0)}$ and $y_{G(n+1)}$ different values, the full range of lines of thrust passing through the hinges and characterized by different distance from the geometric axis of the arch and different shape can be explored. To find the line of thrust passing through the hinges and nearest to the geometric axis, the trial-and-error procedure works as follows. For trial values of $y_{G(n+1)} < y_{G(n)}$ and $y_{G(0)} < y_{G(1)}$, iteratively:

- vector $\{Y_G\}$ is updated and vector $\{W_1\} - [N_{1,2}]\{P_2\}$ is computed accordingly;
- Eq. (B.9) is solved and the unknown $\{P_1\} = \{k\}$ is found;
- the ordinates of the vertices of the line of thrust are calculated, by entering the current value of k into Eq. (B.3);
- the function S in Eq. (A.4) is calculated excluding the ordinates of the vertices P_0 and P_{n+1} of the line of thrust and of the fictitious centroids G_0 and G_{n+1}, that is the equation $S = \sum_{i=1}^{n}(\Delta y_i)^2 = \sum_{i=1}^{n}(y_i - y_{Gi})^2$ is solved for the n points G_i and P_i.

The procedure stops when the values of $y_{G(0)}$ and $y_{G(n+1)}$ correspond to the minimum of the function S and provides the unknown in Eq. (B.9) and the ordinates of the vertices of the thrust line.

Appendix C

- *Conditions of invertibility of Matrix [D]*

The ordinates of the vertices of the thrust line are given by Eq. (7), where vectors $\{R_1\}$, $\{R_2\}$ and $\{R_3\}$ are obtained by the inversion of matrix [D]. The conditions of invertibility of this matrix are discussed in this section.

For clarity, let us consider an arch subject to n point loads and assume that these loads are placed at a constant horizontal distance, i.e. $h_1 = h_2 = \cdots = h_n = \mathrm{h}$ in Eqs. (2) to (5). Accordingly, the matrix $[D] \in \Re^{n \cdot n}$ updates to the form:

$$[D] = \frac{1}{\mathrm{h}} \cdot \begin{bmatrix} 2 & -1 & 0 & 0 \\ -1 & 2 & -1 & 0 \\ \cdots & \cdots & \cdots & \cdots \\ 0 & -1 & 2 & -1 \\ \cdots & \cdots & \cdots & \cdots \\ 0 & 0 & -1 & 2 \end{bmatrix} \tag{C1}$$

that is:

$$[D] = \frac{1}{\mathrm{h}} \cdot \left[\overline{D}\right] \tag{C2}$$

For a chosen value of n, the determinant of matrix [D] is obtained through Eq. (C.3):

$$det[D] = \left(\frac{1}{\mathrm{h}}\right)^n \cdot \left\{ \sum_{i=1}^{n} \overline{d}_{ij} \cdot (-1)^{i+j} \cdot det\left[\overline{D}_{ij}\right] \right\} \tag{C3}$$

where $\left\{\sum_{i=1}^{n} \overline{d}_{ij} \cdot (-1)^{i+j} \cdot det\left[\overline{D}_{ij}\right]\right\}$ is the determinant of the matrix $[\overline{D}]$ computed by using the Laplace expansion along the first row and $\left(\frac{1}{\mathrm{h}}\right)^n$ is the factor that transforms it into the determinant of matrix [D]. In Eq. (C.3), $(-1)^{i+j}\cdot\det\left[\overline{D_{ij}}\right]$ is the cofactor of $\overline{d_{ij}}$ in $[\overline{D_{ij}}]$.

Applying Eq. (C.3) to Eq. (C.1), you get:

$$det[D] = \frac{n+1}{h^n} \tag{C4}$$

To conform to the physical meaning of the problem of the arch, n > 1 and h > 0. Therefore, the determinant of the matrix [D], given by Eq. (C.4), is certainly positive. According to the invertible matrix theorem, having found a nonzero determinant the invertibility condition of matrix [D] is proved.

- *Conditions of invertibility of Matrix [N]*

The minimization procedure leads to the system of three linear equations shown in Eq. (13). The solution of this equation requires the inversion of the submatrix $[N_{1,1}]$ of matrix $[N] \in \Re^{3\cdot 3}$. Note that $[N_{1,1}] = [N]$ for the fixed arch (Eq. (12), $[N_{1,1}] \in \Re^{2\cdot 2}$ for the one-hinged arch (Eq. A.10) and $[N_{1,1}] \in \Re^{1\cdot 1}$ for the two-hinged arch (Eq. (B.8) as well as for the arch on pinned supports (Eq. (20).

The invertible matrix theorem offers a list of equivalent conditions for a square matrix to have an inverse. To discuss the condition of invertibility of matrix $[N_{1,1}]$, we consider the general matrix of order 3 and we apply the Gaussian elimination method to prove that this matrix is of full rank. For this reason and for clarity, we will refer to it hereafter as matrix [N].

The matrix [N], in reduced row echelon form, is shown in Eq. (C.5):

$$\begin{bmatrix} \{R_1\}^2 & \{R_1\}\{R_2\} & \{R_1\}\{R_3\} \\ 0 & (\{R_1\}\{R_2\})(\{R_1\}\{R_3\}) - \{R_1\}^2(\{R_2\}\{R_3\}) & 0 \\ 0 & 0 & (\{R_1\}\{R_3\})(\{R_1\}\{R_2\}) - \{R_1\}^2(\{R_2\}\{R_3\}) \end{bmatrix} \tag{C5}$$

The rank of this matrix is 3 because all its columns are linearly independent. In fact, the first column is non-zero because $\{R_1\}$ is a non-zero vector and, therefore, entry $n_{11} = \{R_1\}^2$ is positive. The second column is non-zero because entry $n_{22} \neq 0$ as a result of the fact that $(\{R_1\}\{R_2\})(\{R_1\}\{R_3\}) \neq \{R_1\}^2(\{R_2\}\{R_3\})$. Similarly, the third column is non-zero because entry $n_{33} \neq 0$ as a result of the fact that $(\{R_1\}\{R_3\})(\{R_1\}\{R_2\}) \neq \{R_1\}^2(\{R_2\}\{R_3\})$.

- *Necessary and sufficient conditions for the existence of a minimum in function S*

The core of the proposed algorithm to detect the thrust line nearest to the geometric axis of the arch consists in computing the minimum of function S (Eq. (8) and Eq. (9), defined as the square of the vertical distances of the vertices of the thrust line from the centroids G_i identified at the intersection points between the lines of action of the loads and the geometric axis.

The necessary condition of existence of a stationary point of a multivariable function is provided by the Fermat's theorem, for which at a stationary point all first-order partial derivatives must be zero. Accordingly, the necessary conditions of function $S = S(k, y_0, y_{n+1})$ are given in Eq. (10) for the fixed arch, Eq. (16) for the arch on pinned supports and for the two-hinged arch, while for the one-hinged arch they are given in Eq. (A.6).

To prove that the stationary point of coordinates (k, y_0, y_{n+1}) given by the equations mentioned above is the minimum of the function, we discuss here the sufficient condition. The sufficient condition for a stationary point to be a minimum of the function requires that the Hessian matrix of the function S, H_S, computed in that point, is positive defined. To prove that the Hessian matrix of the function is positive defined, one can alternatively exploit Sylvester's theorem and Descartes' rule. The Sylvester's theorem, which states that a symmetric squared matrix is positive defined if and only if the determinant of all its principal minors is positive, is used here. So, the Hessian matrix of the function S is computed in Eq. (C.6):

$$[H_S] = \begin{bmatrix} \{R_1\}^2 & \{R_1\}\{R_2\} & \{R_1\}\{R_3\} \\ \{R_1\}\{R_2\} & \{R_2\}^2 & \{R_2\}\{R_3\} \\ \{R_1\}\{R_3\} & \{R_2\}\{R_3\} & \{R_3\}^2 \end{bmatrix} = [H_S{}^{(3)}] \tag{C6}$$

It is worth noting that all entries of this matrix are positive, because all entries of vectors $\{R_1\}$, $\{R_2\}$, $\{R_3\}$ are positive.

Eq. (C.6) is also the principal minor of order 3, $[H_S{}^{(3)}]$ and its determinant is given in Eq. (C.7):

$$\begin{aligned} det\left[H_S{}^{(3)}\right] = {} & \{R_1\}^2\cdot\left[\{R_2\}^2\{R_3\}^2 - (\{R_2\}\{R_3\})(\{R_2\}\{R_3\})\right] - (\{R_1\}\{R_2\})\cdot\left[(\{R_1\}\{R_2\})\{R_3\}^2 - (\{R_1\}\{R_3\})(\{R_2\}\{R_3\})\right] \\ & + (\{R_1\}\{R_3\})\cdot\left[(\{R_1\}\{R_2\})(\{R_2\}\{R_3\}) - (\{R_1\}\{R_3\})\{R_2\}^2\right] \end{aligned} \tag{C7}$$

The principal minors of order 2, $[H_S{}^{(2)}]$, and order 1, $[H_S{}^{(1)}]$, are shown in Eq. (C.8) and Eq. C.10, respectively, and their determinants in Eq. (C.9) and Eq. C.11:

$$[H_S{}^{(2)}] = \begin{bmatrix} \{R_1\}^2 & \{R_1\}\{R_2\} \\ \{R_1\}\{R_2\} & \{R_2\}^2 \end{bmatrix} \tag{C8}$$

$$det\left[H_S{}^{(2)}\right] = \{R_1\}^2\{R_2\}^2 - (\{R_1\}\{R_2\})(\{R_1\}\{R_2\}) \tag{C9}$$

$$[H_S{}^{(1)}] = \left[\{R_1\}^2\right] \qquad 10)$$

$$det\left[H_S{}^{(1)}\right] = \{\mathrm{R}_1\}^2 \tag{11}$$

The determinant of the principal minor $[H_S{}^{(1)}]$ (Eq. C.11) is certainly positive because it is the 2nd power of the nonzero vector $\{\mathrm{R}_1\}$.

The determinant of the principal minor $[H_S{}^{(2)}]$ (Eq. (C.9) is positive because $\{\mathrm{R}_1\}^2\{\mathrm{R}_2\}^2 > (\{\mathrm{R}_1\}\{\mathrm{R}_2\})(\{\mathrm{R}_1\}\{\mathrm{R}_2\})$.

Following the same reasoning as for $[H_S{}^{(2)}]$, the determinant of the principal minor $[H_S{}^{(3)}]$ (Eq. (C.7) is also positive.

References

Bell, W., 1872. On the stresses of rigid arches, continuous beams, and curved structures. Minutes of the Proceedings of the Institution of Civil Engineers 33, 58–126. https://doi.org/10.1680/imotp.1872.22892.

Block, P., Ciblac, T., Ochsendorf, J., 2006. Real-time limit analysis of vaulted masonry buildings. Comput. Struct. 84 (29/30), 1841–1852. https://doi.org/10.1016/j.compstruc.2006.08.002.

Block, P., Ochsendorf, J., 2007. Thrust network analysis: a new methodology for three-dimensional equilibrium. Journal of the International Association for Shell and Spatial Structures 48 (155), 167–173.

Briccoli Bati, S., Fagone, M., Rotunno, T., 2013. Lower bound limit analysis of masonry arches with CFRP reinforcements: a numerical method. J. Compos. Constr. 17 (4), 543–553. https://doi.org/10.1061/(ASCE)CC.1943-5614.0000350.

Cavalagli, N., Gusella, V., Severini, L., 2016. Lateral loads carrying capacity and minimum thickness of circular and pointed masonry arches. Int. J. Mech. Sci. 115–116, 645–656. https://doi.org/10.1016/j.ijmecsci.2016.07.015.

Como, M., Sinopoli, A., 1998. Minimum and maximum thrust states in statics of ancient masonry bridges, in Sinopoli A. (Ed.), Arch Bridges: Hist. Anal. Assess. Maint. Repair, CRC Press, London, pp. 133–138. https://doi.org/10.1201/9781003078494-20.

Del Piero, G., 1998. Limit analysis and no-tension materials. Int. J. Plast. 14 (1/3), 259–271. https://doi.org/10.1016/S0749-6419(97)00055-7.

Dimitri, R., Tornabene, F., 2015. A parametric investigation of the seismic capacity for masonry arches and portals of different shapes. Eng. Fail. Anal. 52, 1–34. https://doi.org/10.1016/j.engfailanal.2015.02.021.

Drucker, D.C., Prager, W., Greenberg, H.J., 1952. Extended limit design theorems for continuous media. Quart. Appl. Math. 9, 381–389. https://doi.org/10.1090/QAM/45573.

Fuller, G., 1875. Curve of equilibrium for a rigid arch under vertical forces. Minutes of the Proceedings of the Institution of Civil Engineers 40, 143–1119. https://doi.org/10.1680/imotp.1875.22708.

Galassi, S., 2023. An alternative approach for limit analysis of masonry arches on moving supports in finite small displacements. Eng. Fail. Anal. 145, 107004 https://doi.org/10.1016/j.engfailanal.2022.107004.

Galassi, S., Tempesta, G., 2023. Numerical procedure for detecting the optimal stress state within the profile of a cracked arch, in: Di Paola, M., Fratini, L., Micari, F., Pirrotta, A. (eds), Theoretical and applied Mechanics - AIMETA2022, Materials Research Proceedings, vol. 26. Materials Research Forum LLC., Millersville PA, USA, pp. 343-348, 2023, Proc. of AIMETA 2022, 4-8 September 2022, Palermo, Italy, pp. 343-348. https://doi.org/10.21741/9781644902431-56.

Galassi, S., Misseri, G., Rovero, L., Tempesta, G., 2020a. Analysis of masonry pointed arches on moving supports: A numeric predictive model and experimental evaluations. In: Lecture Notes in Mechanical Engineering, Springer, Proc. of AIMETA 2019, 15–19 September 2019, Rome, Italy, pp. 2048–2068. https://doi.org/10.1007/978-3-030-41057-5_163.

Galassi, S., Misseri, G., Rovero, L., Tempesta, G., 2018. Failure modes prediction of masonry voussoir arches on moving supports. Eng. Struct. 173, 706–717. https://doi.org/10.1016/j.engstruct.2018.07.015.

Galassi, S., Ruggieri, N., Tempesta, G., 2020b. A novel numerical tool for seismic vulnerability analysis of ruins in archaeological sites. Int. J. Archit. Herit. 14 (1), 1–22. https://doi.org/10.1080/15583058.2018.1492647.

Gáspár, O., Sipos, A.A., Sajtos, I., 2018. Effect of stereotomy on the lower bound value of minimum thickness of semi-circular masonry arches. Int. J. Archit. Herit. 12 (6), 899–921. https://doi.org/10.1080/15583058.2017.1422572.

Gilbert, M., 2001. Ring: a 2d rigid-block analysis program for masonry arch bridges, in: Proc. of International arch bridges conference (ARCH'01), Paris, 19-21 September 2001, pp. 459-464.

Gilbert, M., 2007. Limit analysis applied to masonry arch bridges: state of the art and recent developments, in: P.B. Lourenço, D.B. Oliveira, and A. Portela (Eds.), Proceedings of 5th International Conference on Arch Bridges (ARCH'07), Funchal, Madeira, Portugal, pp. 13-28.

Gregory, D., 1967. Catenaria. Phil Trans 19 (231), 637–652.

Grillanda, N., Chiozzi, A., Milani, G., 2023. Analysis of Gothic Masonry Arches Through a Fully Three-Dimensional Kinematic Limit Analysis Approach, AIP Conference Proceedings 2849,1 (2023), 420005, Proc. of International Conference on Numerical Analysis and Applied Mathematics 2021 (ICNAAM 2021), Rhodes. https://doi.org/10.1063/5.0162075.

Gusella, F., Cluni, F., Gusella, V., 2019. Homogenization of the heterogeneous beam dynamics: the influence of the random Young's modulus mixing law. Compos. B Eng. 167, 608–614. https://doi.org/10.1016/j.compositesb.2019.03.025.

Heyman, J., 1966. The stone skeleton. Int. J. Solids Struct. 2 (2), 249–279. https://doi.org/10.1016/0020-7683(66)90018-7.

Heyman, J., 1969. The safety of masonry arches. Int. J. Mech. Sci. 11 (4), 363–385. https://doi.org/10.1016/0020-7403(69)90070-8.

Heyman, J., 2009. La coupe des pierres, in: Karl-Eugen Kurrer, Werner Lorenz, Volker Wetzk (Eds.), Proc. of the Third International Congress on Construction History, Cottbus, Germany, 20-24 May 2009, pp. 807-812.

Huerta, S.F., 2001. Mechanics of masonry vaults: the equilibrium approach. In: Lourenço, P., Roca, P. (Eds.), Historical Constructions. Possibilities of numerical and experimental techniques, Guimarães, Portugal, pp. 47–69.

Iannuzzo, A., Dell'Endice, A., Van Mele, T., Block, P., 2021. Numerical limit analysis-based modelling of masonry structures subjected to large displacements. Comput. Struct. 242 https://doi.org/10.1016/j.compstruc.2020.106372.

Inglis, C., 1951. Applied Mechanics for Engineers. Cambridge University Press.

Livesley, R., 1978. Limit analysis of structures formed from rigid blocks. Int. J. Numer. Methods Eng. 12 (12), 1853–1871. https://doi.org/10.1002/nme.1620121207.

Makris, N., Alexakis, H., 2013. The effect of stereotomy on the shape of the thrust-line and the minimum thickness of semicircular masonry arches. Arch. Appl. Mech. 83, 1511–1533. https://doi.org/10.1007/s00419-013-0763-4.

Marmo, F., 2021. ArchLab: A MATLAB tool for the Thrust Line Analysis of masonry arches. Curved and Layer. Struct. 8 (1), 26–35. https://doi.org/10.1515/cls-2021-0003.

Marmo, F., Rosati, L., 2017. Reformulation and extension of the thrust network analysis. Comput. Struct. 182, 104–118. https://doi.org/10.1016/j.compstruc.2016.11.016.

Marmo, F., Masi, D., Mase, D., Rosati, L., 2019. Thrust network analysis of masonry vaults. International Journal of Masonry Research and Innovation 4 (1/2), 64–77. https://doi.org/10.1504/IJMRI.2019.096828.

Mèry, E., 1840. Mémoire sur l'équilibre des voutes en berceau. Annales Des Ponts et Chaussées X(1), 50–70.

Milani, E., Milani, G., Tralli, A., 2008. Limit analysis of masonry vaults by means of curved shell finite elements and homogenization. Int. J. Solids Struct. 45, 5258–5288. https://doi.org/10.1016/j.ijsolstr.2008.05.019.

Moseley, H., 1833. On a new principle in statics called the principle of least pressure. The London, Edinburgh, and Dublin Philosophical Magazine and Journal of Science 3 (16), 285–1228.

Ng, H.K., Fairfield, C.A., 2004. Modifying the mechanism method of masonry arch bridge analysis. Constr. Build. Mater. 18 (2), 91–97. https://doi.org/10.1016/j.conbuildmat.2003.08.015.

O'Dwyer, D., 1999. Funicular analysis of masonry vaults. Comput. Struct. 73 (1), 187–197. https://doi.org/10.1016/S0045-7949(98)00279-X.

Paradiso, M., Galassi, S., Sinicropi, D., 2014. Stabilità di archi e volte in muratura: metodi tradizionali e calcolo automatico. In: Villegas, L., Lombillo, I., Liano, C., Blanco, H. (Eds.), Patologia Della Costruccion. Tecnologia de la Rehabilitacion y Gestion del Patrimonio, Gráficas Iguña, S.A., Santander, Spain, pp. 960–969.

Pippard, A.J.S., Ashby, R., 1939. An experimental study of the voussoir arch. J. Inst. Civil. Eng. 10 (3), 383–404. https://doi.org/10.1680/ijoti.1939.14554.

Pugi, F., Galassi, S., 2013. Seismic analysis of masonry voussoir arches according to the Italian building code. Ingegneria Sismica 30 (3), 33–55.

Riveiro, B., Morer, P., Arias, P., de Arteaga, I., 2011. Terrestrial laser scanning and limit analysis of masonry arch bridges. Constr. Build. Mater. 25 (4), 1726–1735. https://doi.org/10.1016/j.conbuildmat.2010.11.094.

Smars, P., 2010. Kinematic stability of masonry arches. Adv. Mater. Res. 133, 429–434. https://doi.org/10.4028/www.scientific.net/AMR.133-134.429.

Stockdale, G., Tiberti, S., Camilletti, D., Sferrazza Papa, G., Basshofi Habieb, A., Bertolesi, E., Milani, G., Casolo, S., 2018. Kinematic collapse load calculator: circular arches. SoftwareX 7, 174–179. https://doi.org/10.1016/j.softx.2018.05.006.

Tempesta, G., Galassi, S., 2019. Safety evaluation of masonry arches. A numerical procedure based on the thrust line nearest to the geometric axis. Int. J. Mech. Sci. 155, 206–221. https://doi.org/10.1016/j.ijmecsci.2019.02.036.

Tralli, A., Chiozzi, A., Grillanda, N., Milani, G., 2020. Masonry structures in the presence of foundation settlements and unilateral contact problems. Int. J. Solids Struct. 191–192, 187–201. https://doi.org/10.1016/j.ijsolstr.2019.12.005.

Villarceau, Y., 1854. L'établissement des arches de pont, Institut de France. Académie Des Sciences, Mémoires Présentés Par Divers Savants 12, 506–822.

Winkler, E., 1867. Die Lebre von der Elasticitat und Festigkeit. Dominicus, Prague.

Zampieri, P., Simoncello, N., Pellegrino, C., 2018a. Structural behavior of masonry arch with no-horizontal springing settlement. Frattura Ed Integrità Strutturale 12 (43), 182–190. https://doi.org/10.3221/IGF-ESIS.43.14.

Zampieri, P., Cavalagli, N., Gusella, V., Pellegrino, C., 2018b. Collapse displacements of masonry arch with geometric uncertainties on spreading supports. Comput. Struct. 208, 118–129. https://doi.org/10.1016/j.compstruc.2018.07.001.

Zampieri, P., Simoncello, N., Pellegrino, C., 2019a. Seismic capacity of masonry arches with irregular abutments and arch thickness. Constr. Build. Mater. 201, 786–806. https://doi.org/10.1016/j.conbuildmat.2018.12.063.

Zampieri, P., Amoroso, M., Pellegrino, C., 2019b. The masonry buttressed arch on spreading support. Structures 20, 226–236. https://doi.org/10.1016/j.istruc.2019.03.008.